

# Thermo-mechanical Buckling of Curvilinearly Stiffened Variable Angle Tow Laminated Panels

Wei Zhao\*, Karanpreet Singh† and Rakesh K. Kapania‡

*Virginia Polytechnic Institute and State University, Blacksburg, VA, 24061*

Variable-Angle-Tow (VAT) laminates are known for their ability to redistribute the in-plane stress resultants so as to improve their structural buckling response. Curvilinear stiffeners are known to be able to tailor the buckling mode shape to increase the buckling load of a panel. This paper studies the thermo-mechanical buckling of stiffened composite panels with both the VAT laminates and curvilinear stiffeners. Considering the meshing difficulties for analyzing the curvilinearly stiffened VAT laminated plate due to both spatially dependent fiber ply orientation and arbitrarily shaped stiffeners when using finite element analysis, the modeling of a curvilinearly stiffened VAT laminated panel is treated separately in the present work without the need to place finite element nodes along the stiffener/plate and stiffener/stiffener interfaces. The degrees of freedom for the stiffeners are transformed to those of the plate, through the displacement compatibility conditions at the stiffener/plate and stiffener/stiffener interfaces via finite element interpolation. Results show that the present method can accurately predict the buckling behaviors of VAT laminates under both thermal and mechanical loads. Parametric studies show that either VAT laminates or curvilinear stiffeners alone can improve the buckling temperature and the buckling load to higher values than those obtained using the traditional stiffened laminates using straight-fiber laminates and straight stiffeners. Optimization studies using the present method along with the particle swarm optimization found that the combination of curvilinear stiffeners and VAT laminates for the plate can improve the total buckling responses in the presence of either thermal or mechanical loads by

---

\*Post-doctoral Fellow, Kevin T. Crofton Department of Aerospace and Ocean Engineering, AIAA Member, weizhao@vt.edu

†Graduate Research Assistant, Kevin T. Crofton Department of Aerospace and Ocean Engineering, AIAA Student Member, kasingh@vt.edu

‡Norris and Wendy Mitchell Endowed Professor, Kevin T. Crofton Department of Aerospace and Ocean Engineering, AIAA Associate Fellow, rkapania@vt.edu

up to 28% as compared to that using straight-fiber laminates and curvilinear stiffeners.

## Nomenclature

$A_s$	stiffener cross-sectional area
$a$	length of the composite panel
$\mathbf{B}$	displacement-strain matrix
$b$	width of the composite panel
$b_s$	width of the composite stiffener
$\mathbf{D}$	constitutive matrix giving stress resultant-strain relations
$d_p$	panel displacements
$d_s$	stiffener displacements described in a local coordinate system
$d_{sg}$	stiffener displacements described in the global coordinate system
$e$	eccentricity of the stiffener, $e = \frac{1}{2}(t_p + h_s)$
$G_s J_s$	stiffener effective torsional rigidity
$h_s$	stiffener height
$I_n, I_b$	stiffener second moment of area about the $n$ and $b$ axis, respectively
$\mathbf{J}$	Jacobian of the coordinate transformation
$K$	shear correction factor, $K = 5/6$
$\mathbf{K}_p$	panel elastic stiffness matrix
$\mathbf{K}_s$	stiffener elastic stiffness matrix
$\mathbf{K}_{Gp}$	panel geometric stiffness matrix
$\mathbf{K}_{Gs}$	stiffener geometric stiffness matrix
$\mathbf{N}_{sp}$	shape functions to represent stiffener nodal displacement using panel nodal displacements
$N_{xx}, N_{yy}, N_{xy}$	the two in-plane normal loads and the in-plane shear load, N/mm, respectively
$N_{cr,p}$	the critical buckling load for the unstiffened cross-ply laminated plate, N/mm
$N_{cr}$	the critical buckling load for the stiffened laminated plate, N/mm
$R$	the radius of curvature of the curved stiffener
$\mathbf{T}_s$	transformation matrix
$t_p$	panel thickness
$\Gamma$	stiffener arch length domain
$\Omega$	panel area domain
$\xi, \eta$	natural coordinates
$\varepsilon, \sigma$	strain and stress, respectively
$\alpha$	angle between the stiffener tangential direction $t$ and the global $x$ axis
$\boldsymbol{\sigma}^0$	external in-plane stress vector
$\Delta\varepsilon$	parameter for the stiffener placement
$\Delta T$	temperature change
$\hat{T}$	temperature change gradient
$\theta$	variable fiber ply angle

## I. Introduction

High-speed air-vehicles and spacecraft are subjected to severe environment during their normal operations, such as due to aerodynamic heating. The importance of thermal effects on aircraft design has received attention as early as during the World War II [1]. Both material degradation in high temperature and thermal stress due to an restrained thermal expansion generated at an elevated temperature may cause a structure failure and reduce both the safety and the life of a super/hypersonic aircraft.

Composite structures have been widely used in aerospace vehicles due to their higher strength-to-weight ratio and higher heat resistant properties [2]. The innovative manufacturing technologies in composites, such as, Automated Fiber Placement (AFP) [3] have made it possible to fabricate spatially-varying angle fiber-ply laminate for composites to further improve the structural performances [4]. Additionally, the fabrication technologies using Resin Transfer Molding (RTM) [3] and Electronic Beam Free Form Fabrication (EBF3) [5] for integrally stiffened panels leads to a further improvement in structural performance. The development in the manufacturing technologies along with the super/hypersonic flight induced thermal effects and complex loads for the aircraft local wing panels lead to an interest in studying the structural performance of stiffened VAT laminated panels with arbitrarily shaped stiffeners subjected to both mechanical and thermal loads.

For local panels used in a hypersonic vehicle, both thermal and mechanical loads are generated at the panels' edges. Thermal buckling is induced by the temperature change due to the aerodynamic heating and the restrained thermal expansion [6]. This phenomena is common for restrained panels of re-entry launch vehicles. Various approaches were studied for performing thermal buckling of composite plates and shells with straight fibers [7–11], and thermal buckling of structures made of functionally graded materials [12, 13]. A recent work on thermal buckling analysis of VAT laminated plate [14] showed that an increased buckling load can be obtained by tailoring the curved fiber ply path in the panel as compared to that using straight-fiber laminates. IJsselmuiden *et al.* [15] studied thermo-mechanical buckling optimization of VAT laminated panels. They found that the proper tailoring of both the stiffness and thermal properties of a VAT laminated plate can increase the buckling loads significantly as compared to the quasi-isotropic laminated panels. All these works demonstrate the benefits of using VAT laminates to improve the buckling response of such panels under both thermal and mechanical loads.

Static and buckling analyses of VAT laminated panels have received considerable research interest during last several decades. Gürdal *et al.* [16] found that the VAT laminates can tailor the in-plane stress resultants to a favorable one that can improve the buckling load. Based on this finding by Gürdal *et al.* [16], several optimization studies on buckling maximization of a VAT laminated plate have been conducted. Setoodeh *et al.* [17] optimized the fiber path for VAT laminated plates using finite element method and the gradient-based approach. The optimization results showed a significant improvement in the buckling loads of a VAT

laminated plate as compared to a plate with straight fibers. IJsselmuiden *et al.* [18] studied buckling load maximization of VAT laminated panels using the finite element method and lamination parameters. They showed that a significant improvement in the buckling loads of a plate with VAT laminates as compared to that with straight fibers. These optimization studies [17, 18] found that it is the in-plane load redistribution through tailoring the fiber path orientations that leads to an improvement in the buckling load for the VAT laminated structures. Wu *et al.* [19] used the Rayleigh-Ritz approach for the buckling analysis and a genetic algorithm as the optimizer to perform the buckling load maximization. A nonlinear distribution of fiber ply angles was considered to achieve a maximum buckling load which is close to that obtained using lamination parameters as studied by IJsselmuiden *et al.* [18].

Additionally, stiffeners are added to further improve the buckling load of VAT laminated plates by modifying the buckling mode wavelength. Zhao and Kapania [20] studied the buckling of curvilinearly stiffened composite plate in the presence of both the in-plane axial and shear loads. The parametric studies on their work reveal that it is possible to improve the buckling responses in terms of tailoring the stiffener shapes on modifying the buckling mode shape for improving the buckling load. Coburn *et al.* [21] used the Rayleigh-Ritz method to study both the local and global buckling responses of stiffened VAT laminated plates. Zhao and Kapania [22] studied the buckling of stiffened VAT laminated plates subjected to various linearly varying in-plane loads. Parametric studies in that work [22] showed that the capability of the in-plane stress redistribution of using VAT laminates can improve the buckling responses for both unstiffened and stiffened laminated plates. Due to the ability of modifying the buckling mode shape using curvilinear stiffeners and the in-plane stress redistribution of using VAT laminates for a plate, Stanford and Jutte [23] studied the aircraft wing box design using both curvilinear stiffeners and tow-steered composites simultaneously for wing panel design. Their results showed that an integrated design leads to a larger weight reduction as compared to the design of using them independently. Singh and Kapania [24] studied the buckling maximization for a composite panel with both curvilinear fibers and curvilinear stiffeners. Their research showed a substantial benefit of using the two technologies simultaneously for maximizing the panel buckling loads. These two representative optimization results [23, 24] drive the research interest to study the buckling response of the VAT laminated plate with curvilinear stiffeners in the presence of both thermal and mechanical loads. Considering the manufacturing constraints of fabricating the laminated stiffeners that cross each other, without a loss of generality, the stiffener is modeled as an orthotropic beam.

For studying the structural responses of the stiffened VAT laminates with arbitrarily shaped stiffeners, both spatially dependent fiber ply orientation and arbitrarily shaped stiffeners could lead to difficulties for generating mesh or obtaining a converged mesh for such structures when using a finite element analysis. A previously developed curvilinearly stiffened panel design optimization framework, EBF3PanelOpt [25] by Mulani, *et al.*, used a commercially available FEA package, MSC PATRAN, to mesh such structures, which requires placing nodes at the stiffener/plate and stiffener/stiffener interfaces. An increase in the stiffener number increases the number of design variables and the difficulty in meshing such structures with many arbitrarily shaped stiffeners, it was recommended to use a

maximum of six stiffeners in shape optimization when using EBF3PanelOpt [25].

An emerging technology developed in MSC PATRAN/NASTRAN, named glue contact [26], which is an automated technique that can be used to merge two surfaces together using multipoint constraints. This technology releases the constraint in placing nodes at the stiffener/plate interfaces when meshing the curvilinearly stiffened structures for a finite element analysis. Levia [27] used this technology to study the effect of curvilinear spars and ribs in aircraft wing box design to avoid a repeated meshing work during shape optimization. Singh and Kapania [28] used this technology for studying the mechanical buckling optimization of curvilinearly stiffened plates with VAT laminates. However, the optimization problem becomes complex in pre-processing of such structures when there are many arbitrarily shaped stiffeners as the common nodes at the stiffener/stiffener interfaces still should be considered. The number and shape of curvilinear stiffeners increase the difficulty of meshing such structures for performing finite element analysis even when using the glue contact.

Additionally, glue contact is very sensitive to the offsets and gaps between the two models that are to be joined together. Along with some other limitations, such as those pointed out by Ahlbert [29], the glue contact could affect the accuracy of the analysis results or limit the design space in optimizing the stiffener shape for a stiffened structure. In view of these limitations of glue contact technique for conducting shape optimization of curvilinearly stiffened plates, this paper uses an attractive, efficient finite element approach developed by Zhao and Kapania [20, 22] for studying the buckling responses of a stiffened VAT laminated plate with arbitrarily shaped stiffeners. The present approach obviates the need for placing nodes at both the stiffener/plate and stiffener/stiffener interfaces, which avoids a repeated meshing of the stiffened plate in the shape optimization for determining the optimal stiffener shape. The finite element method is used here so that the developed method can compute the objective function and the constraints for use in any stiffened panel design optimization framework, e.g., EBF3PanelOpt [25]. On the other hand, the finite element method works for any shaped panel with any sets of boundary conditions. Additionally, the present method integrates the stiffness matrix for the VAT laminated panel, wherein the fiber ply orientation for each layer is evaluated for each element.

The paper is organized as follows: Section II derives the elastic stiffness and geometric stiffness matrices for the curvilinearly stiffened VAT laminated plate considering the thermal effect, and presents the approximation of the stiffener displacement in terms of the panel's displacement for transforming the stiffeners' elastic and geometric stiffness to those for the panel. Section III presents a geometry parameterization of an arbitrarily shaped stiffener using Hobby spline [30]. Convergence and verification studies regarding the thermal buckling of both straight-fiber and VAT laminated plates are conducted in Section IV. Section V presents verifications on thermal buckling of curvilinearly stiffened composite laminated plates and conducts parametric and optimization studies on thermal buckling of stiffened plates with both VAT laminates and arbitrarily shaped stiffeners. Section VI presents parametric and optimization studies on mechanical buckling of the stiffened plates in the presence of in-plane axial load in terms of both VAT laminates and stiffener shape. The last section, VII, presents concluding remarks.

## II. Formulations

### A. Motion of Tow-steered Laminated Plate

Consider a curvilinearly stiffened panel as shown in Fig. 1a. The panel middle plane  $Oxy$  is chosen as the reference plane of the global coordinate system. The composite panel has the length, width and thickness denoted as  $a$ ,  $b$  and  $t_p$ , respectively. The first-order shear deformation displacement is considered for modeling the plate based on the Mindlin plate theory. Linearly distributed temperature can be considered along the thickness direction for the stiffened panel as shown in Fig. 1b. For the temperature gradient along the laminated panel thickness, normally the temperature decreases from the bottom side to the upper side as shown in Fig. 1b. It is assumed that the temperature changes vary from  $\Delta T_b$  to  $\Delta T_u$  in the panel and from  $\Delta T_m$  to  $\Delta T_u$  in the stiffener. When  $\Delta T_b = \Delta T_m = \Delta T_u$ , a uniform temperature change is obtained in the structure. The degradation of material properties with temperature is not considered in the present work.

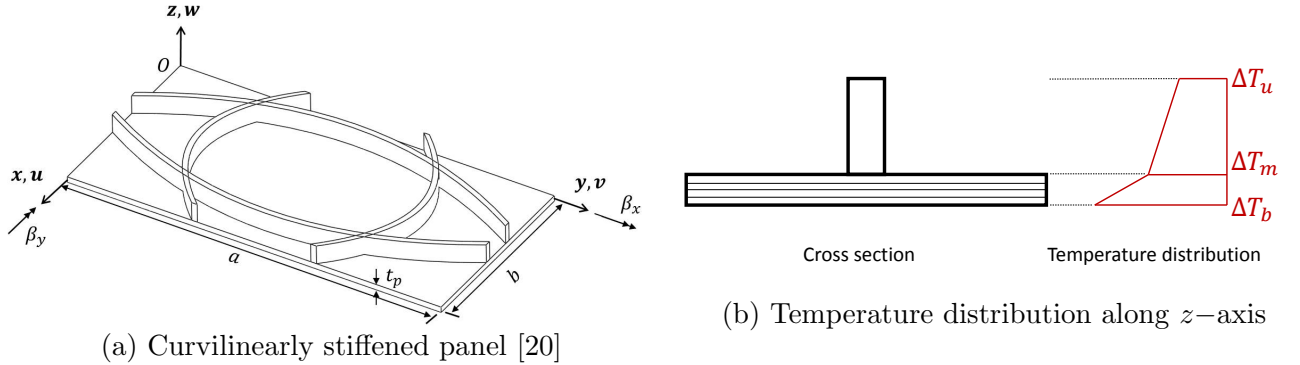


Figure 1: Curvilinearly stiffened panel and temperature distribution

For the VAT laminates, there are several parameterizations available to describe the spatially dependent fiber ply orientations, such as linear variation based flow path [4, 16, 31], the Lagrange polynomials method based nonlinear fiber orientations [19, 21] and B-spline based expression [32, 33]. Considering that the scope of the present paper is to study the effect of VAT laminates and curvilinear stiffeners on the structural's buckling responses, for simplicity, a linear, 1-D variation of a reference fiber path is considered. This linear variation along the panel length direction, *i.e.*  $x$ -axis, can be given as [4]:

$$\theta(x) = 2(\Theta_1 - \Theta_0) \left| \frac{x}{a} \right| + \Theta_0 = (\Theta_1 - \Theta_0) |\bar{x}| + \Theta_0 \quad (1)$$

where  $\Theta_0$  and  $\Theta_1$  are fiber ply orientations at two prescribed locations,  $\bar{x} = 0$  and  $|\bar{x}| = 1$ , respectively, as shown in Fig. 2. The linear variation of the fiber ply orientation is considered and  $\bar{x}$  is a normalized length used in the natural coordinate system ranging from -1 to 1. The laminate configuration for the VAT laminates is characterised as  $[\langle \Theta_0 | \Theta_1 \rangle_k]_{AS}$  where  $k$  is the number of layers and *AS* means antisymmetric laminates.

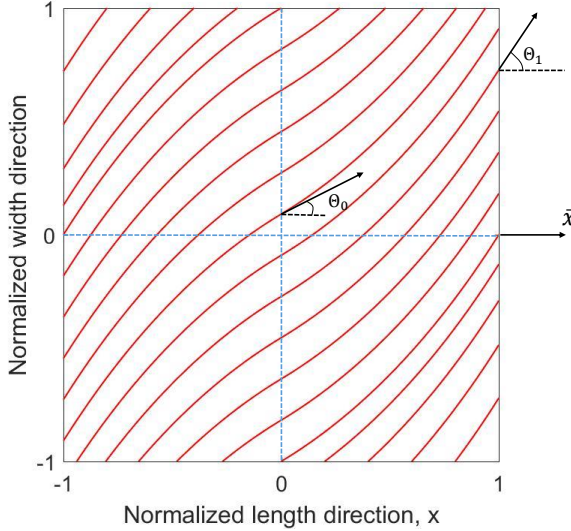


Figure 2: Parameterization of one-layer fiber ply orientation for a VAT laminated plate,  $\langle 30^\circ | 60^\circ \rangle$

Note that the thermal stresses are not caused by external loads but the restrained thermal expansions. The stress-strain relation for each layer for each element described in the global coordinate system, say  $k^{\text{th}}$  layer [34, 35], is:

$$\begin{Bmatrix} \sigma_x \\ \sigma_y \\ \tau_{xy} \end{Bmatrix}^k = \begin{bmatrix} \bar{Q}_{11}[\theta(\bar{x})] & \bar{Q}_{12}[\theta(\bar{x})] & \bar{Q}_{16}[\theta(\bar{x})] \\ \bar{Q}_{12}[\theta(\bar{x})] & \bar{Q}_{22}[\theta(\bar{x})] & \bar{Q}_{26}[\theta(\bar{x})] \\ \bar{Q}_{16}[\theta(\bar{x})] & \bar{Q}_{26}[\theta(\bar{x})] & \bar{Q}_{66}[\theta(\bar{x})] \end{bmatrix}^k \begin{Bmatrix} \varepsilon_x - \alpha_x[\theta(\bar{x})]\Delta T(z) \\ \varepsilon_y - \alpha_y[\theta(\bar{x})]\Delta T(z) \\ \gamma_{xy} - \alpha_{xy}[\theta(\bar{x})]\Delta T(z) \end{Bmatrix} \quad (2)$$

where  $\alpha_x$ ,  $\alpha_y$  and  $\alpha_{xy}$  are thermal expansion coefficients described in the global coordinate system.  $\Delta T$  is the temperature gradient at a certain point along the  $z$ -axis. For the panel, the temperature change is assumed to be  $\Delta T = \Delta T_b + k_1 \times z$ . When  $k_1 = 0$ , a uniform temperature change along the panel thickness direction can be obtained.

Integrating stress given in Eq. (2) over the panel thickness, along with an external load distribution,  $\mathbf{F}^0 = \{N_x^0, \dots, M_{xy}^0\}^T$ , applied at panel edges of the middle plane, one can obtain:

$$\begin{Bmatrix} N_x \\ N_y \\ N_{xy} \\ M_x \\ M_y \\ M_{xy} \end{Bmatrix} = \begin{bmatrix} \bar{A}_{11} & \bar{A}_{12} & \bar{A}_{16} & \bar{B}_{11} & \bar{B}_{12} & \bar{B}_{16} \\ \bar{A}_{12} & \bar{A}_{22} & \bar{A}_{26} & \bar{B}_{12} & \bar{B}_{22} & \bar{B}_{26} \\ \bar{A}_{16} & \bar{A}_{26} & \bar{A}_{66} & \bar{B}_{16} & \bar{B}_{26} & \bar{B}_{66} \\ \bar{B}_{11} & \bar{B}_{12} & \bar{B}_{16} & \bar{D}_{11} & \bar{D}_{12} & \bar{D}_{16} \\ \bar{B}_{12} & \bar{B}_{22} & \bar{B}_{26} & \bar{D}_{12} & \bar{D}_{22} & \bar{D}_{26} \\ \bar{B}_{16} & \bar{B}_{26} & \bar{B}_{66} & \bar{D}_{16} & \bar{D}_{26} & \bar{D}_{66} \end{bmatrix} \begin{Bmatrix} \varepsilon_x^0 \\ \varepsilon_y^0 \\ \gamma_{xy}^0 \\ \kappa_x^0 \\ \kappa_y^0 \\ \kappa_{xy}^0 \end{Bmatrix} - \begin{Bmatrix} N_x^{\Delta T} \\ N_y^{\Delta T} \\ N_{xy}^{\Delta T} \\ M_x^{\Delta T} \\ M_y^{\Delta T} \\ M_{xy}^{\Delta T} \end{Bmatrix} - \begin{Bmatrix} N_x^0 \\ N_y^0 \\ N_{xy}^0 \\ M_x^0 \\ M_y^0 \\ M_{xy}^0 \end{Bmatrix} \quad (3)$$

The thermal stress-resultant,  $\mathbf{F}^{\Delta T} = \{\mathbf{N}^{\Delta T} \mathbf{M}^{\Delta T}\}^T$ , can be obtained by integrating the thermal stress given in Eq. (2) over the panel thickness:

$$\begin{aligned} \{\mathbf{N}^{\Delta T} \mathbf{M}^{\Delta T}\}^T &= \sum_{k=1}^{N_{ply}} \int_{z_k}^{z_{k+1}} \{1, z\} \bar{\mathbf{Q}}[\theta(\bar{x})] \left\{ \begin{array}{c} -\alpha_x[\theta(\bar{x})]\Delta T(z) \\ -\alpha_y[\theta(\bar{x})]\Delta T(z) \\ -\alpha_{xy}[\theta(\bar{x})]\Delta T(z) \end{array} \right\}^k dz \\ &= - \sum_{k=1}^{N_{ply}} \int_{z_k}^{z_{k+1}} \{1, z\} \bar{\mathbf{Q}}[\theta(\bar{x})] \left\{ \begin{array}{c} \alpha_x[\theta(\bar{x})](\Delta T_b + k_1 \times z) \\ \alpha_y[\theta(\bar{x})](\Delta T_b + k_1 \times z) \\ \alpha_{xy}[\theta(\bar{x})](\Delta T_b + k_1 \times z) \end{array} \right\}^k dz \quad (4) \\ &= - \sum_{k=1}^{N_{ply}} \int_{z_k}^{z_{k+1}} \{1, z\} \bar{\mathbf{Q}}[\theta(\bar{x})] \bar{\boldsymbol{\alpha}}^k[\theta(\bar{x})](\Delta T_b + k_1 \times z) dz \end{aligned}$$

where  $\bar{\boldsymbol{\alpha}}$  is the vector for thermal expansion coefficients described in the global coordinate system. Note that the thermal stress described in the global coordinate system vary from element to element due to the spatially-varying fiber path angle laminates.

The constitutive matrix,  $\mathbf{ABD}$ , in Eq. (3) can be found in Ref. [36]. Note that the  $\mathbf{ABD}$  matrix for the VAT laminated plates is spatially dependent since the fiber ply orientation changes with the element for each layer. For each layer, the fiber ply orientation evaluated at the center of each element is considered for computing the constitutive matrix for each element.

Equation (3) shows that the in-plane stress resultants for a plate depending on both mechanical in-plane loads and the temperature changes. As there are many different combinations of these two loads, for simplicity, we are going to study the buckling of the stiffened plate subjected to the thermal induced expansion and the mechanical in-plane loads separately. For a linear buckling analysis performed here, a linear static analysis is first conducted for the structure to determine the stress distribution among the structure for geometric stiffness. The thermal stresses due to the temperature change is added to the mechanical stress obtained from the linear static analysis for the VAT laminated plates subjected to external applied in-plane loads and/or initial displacements.

## B. Stiffener Motion

Consider a curved blade stiffener as shown in Fig. 3. The stiffener is modeled using composite beam elements, based on Timoshenko beam theory. The stiffener shape is arbitrarily, curvilinear. The solid rectangular cross section of the stiffener has width and height denoted as  $b_s$  and  $h_s$ , respectively. The stiffener eccentricity,  $e$ , is defined as a measure of the offset between the stiffener neutral line and the panel middle plane,  $e = \frac{1}{2}(h_s + t_p)$ . When the stiffener neutral line coincides with the panel middle plane,  $e = 0$ , we called the plate as a concentrically stiffened panel. The warping of the stiffener is ignored in this study because the stiffener motion is governed by the plate. A local curvilinear coordinate system  $tnb$  is

used to describe the motion of the curved stiffener as shown in Fig. 3.

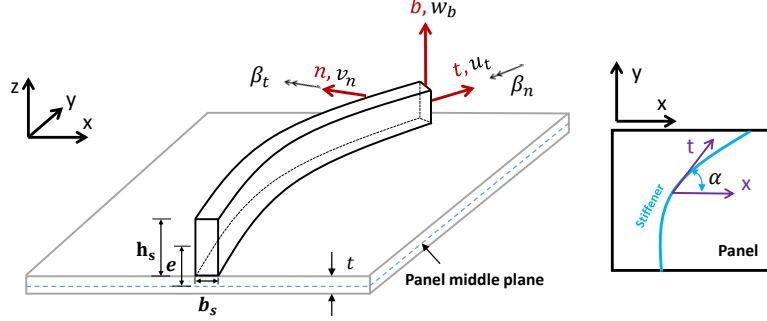


Figure 3: Definitions of displacement and local coordinate system for curved stiffeners

It should be pointed out that the stiffener is only restrained in its longitudinal direction and the other directions are free. Hence, the thermal strain along the principal direction, 1-axis, is considered. The stress-strain relation for an orthotropic stiffener is given as:

$$\left\{ \begin{array}{l} \sigma_{tt} \\ \sigma_{nn} \\ \sigma_{bb} \\ \tau_{nb} \\ \tau_{tb} \\ \tau_{tn} \end{array} \right\} = \left[ \begin{array}{cccccc} C_{11} & C_{12} & C_{13} & 0 & 0 & 0 \\ C_{12} & C_{22} & C_{23} & 0 & 0 & 0 \\ C_{13} & C_{23} & C_{33} & 0 & 0 & 0 \\ 0 & 0 & 0 & C_{44} & 0 & 0 \\ 0 & 0 & 0 & 0 & C_{55} & 0 \\ 0 & 0 & 0 & 0 & 0 & C_{66} \end{array} \right] \left\{ \begin{array}{l} \varepsilon_{tt} - \alpha_1 \Delta T \\ \varepsilon_{nn} \\ \varepsilon_{bb} \\ \gamma_{nb} \\ \gamma_{tb} \\ \gamma_{tn} \end{array} \right\} \quad (5)$$

where the  $C_{ij}$  can be found in Ref. [37].

The constitutive equation shown in above Eq. (5) for the beam can be further simplified based on the stress assumptions for a 3D beam. All stresses at the beam in the local coordinate system  $t$  $n$  $b$  are presumed to be negligible except  $\sigma_t(\sigma_{tt})$ ,  $\tau_n(\tau_{tn})$  and  $\tau_b(\tau_{tb})$ . However, all strains are not assumed to be zero. The stress-strain relation for the stiffener can be expressed as:

$$\left\{ \begin{array}{l} \sigma_t \\ \tau_n \\ \tau_b \end{array} \right\} = \left[ \begin{array}{ccc} \bar{C}_{11} & 0 & 0 \\ 0 & \bar{C}_{66} & 0 \\ 0 & 0 & \bar{C}_{55} \end{array} \right] \left\{ \begin{array}{l} \varepsilon_t \\ \gamma_n \\ \gamma_b \end{array} \right\} + \left\{ \begin{array}{l} -\bar{C}_{11}\alpha_1 \Delta T \\ 0 \\ 0 \end{array} \right\} \quad (6)$$

where

$$\begin{aligned} \bar{C}_{55} &= C_{55}, \quad \bar{C}_{66} = C_{66} \\ \bar{C}_{11} &= \frac{C_{13}^2 C_{22} - 2C_{12}C_{13}C_{23} + C_{11}C_{23}^2 + C_{12}^2 C_{33} - C_{11}C_{22}C_{33}}{C_{23}^2 - C_{22}C_{33}} \end{aligned}$$

The stress resultants,  $\{N_t, V_b, V_n, M_t, T_n\}^T$ , can be obtained by integrating stress as shown in Eq. (6) over the stiffener cross section. Recall that the generalized strain for the stiffener is  $\boldsymbol{\varepsilon}_s = \{\varepsilon_t^0, \gamma_n^0, \gamma_b^0, \kappa_t^0, \kappa_n^0\}^T$ . The relation between the stress-resultants and strains is available in [22, 38].

The strain energy,  $U_s$ , of the composite stiffener can be expressed as:

$$U_s = \frac{1}{2} \int_{\Gamma} \boldsymbol{\varepsilon}_s^T \mathbf{D}_s^T \boldsymbol{\varepsilon}_s d\Gamma = \frac{1}{2} \int_{\Gamma} \mathbf{d}_p^T \mathbf{N}_{sp}^T \mathbf{T}_s^T \mathbf{B}_s^T \mathbf{D}_s \mathbf{B}_s \mathbf{T}_s \mathbf{N}_{sp} \mathbf{d}_p d\Gamma \quad (7)$$

where  $\Gamma$  is used to describe the stiffener length domain;  $\mathbf{T}_s$  is a transformation matrix which relates the stiffener displacement field,  $\mathbf{d}_s$ , described in the local coordinate system *tnb* and the stiffener displacement field,  $\mathbf{d}_{sg}$ , described in the global coordinate system *xyz*,  $\mathbf{d}_s = \mathbf{T}_s \mathbf{d}_{sg}$ ;  $\mathbf{B}_s$  and  $\mathbf{D}_s$  are the displacement-strain matrix and the stress resultant-strain constitutive matrix, respectively, for the stiffener. The expression for those matrices are given in Ref. [20]. The stiffener element nodal displacements are approximated using those for the plate,  $\mathbf{d}_{sg} = \mathbf{N}_{sp} \mathbf{d}_p$  where  $\mathbf{N}_{sp}$  is briefly shown in Section C.

For buckling analysis, the potential for the stiffener,  $W_s$ , subjected to axial stress, can be expressed as:

$$W_s = -\frac{1}{2} \int_{\Gamma} \mathbf{d}_p^T \mathbf{N}_{sp}^T \mathbf{T}_s^T (\mathbf{B}_s^{NL})^T \boldsymbol{\sigma}_s \mathbf{B}_s^{NL} \mathbf{T}_s \mathbf{N}_{sp} \mathbf{d}_p d\Gamma \quad (8)$$

where  $\boldsymbol{\sigma}_s$  is the total stress matrix; the expressions for  $\mathbf{B}_s^{NL}$  is given in Ref. [20]. The total stress matrix for stiffeners under a uniform temperature change and mechanical load is:

$$\boldsymbol{\sigma}_s = (-\bar{C}_{11}\alpha_1\Delta T + \sigma_t) \begin{bmatrix} A_s & 0 & 0 \\ 0 & I_n & 0 \\ 0 & 0 & I_n \end{bmatrix} \quad (9)$$

where  $\alpha_1$  and  $\Delta T$  is thermal expansion coefficient and temperature gradient, respectively. And  $\sigma_t$  is the mechanical in-plane axial stress for the stiffener. Note that the stiffener is made of orthotropic material, the value of  $\alpha_1$  is not spatially dependent.

### C. Stiffener displacement approximation

Considering that a fine mesh is often used for a curvilinearly stiffened VAT laminated plate due to both spatial dependent fiber ply orientation and arbitrarily shape stiffeners when using a traditional finite element method, instead of placing common nodes at the plate/stiffener and stiffener/stiffener interfaces, we model the stiffeners and the plate separately in this paper. The transformation matrix  $\mathbf{N}_{sp}$  is used to approximate the stiffener displacement in terms of the plate displacement based on the finite element shape functions for the isoparametric elements. The stiffness and mass matrices for the stiffeners can be transformed to that for the plate. The matrix of  $\mathbf{N}_{sp}$  can be computed using the geometry field for both

the plate and the stiffeners. This method was studied in detail in our previous work [20]. For completeness, a brief summary of the computation of matrix  $\mathbf{N}_{sp}$  is presented.

Figure 4 shows the  $j$ -th beam element, which is used to model the stiffener, passing through the  $i$ -th plate element. Both the displacement and geometry expressions for the node of the  $j$ -th beam element can be approximated in terms of those for the eight nodes of the  $i$ -th plate element based on the isoparametric elements used in the finite element method. Hence, the nodal displacement and geometry for each node ( $m = 1, 2, 3$ ) of the  $j$ -th beam element can be expressed as:

$$d_{sg,j}^m = \sum_{k=1}^8 N_{p,i}^k(\xi_{s,j}^m, \eta_{s,j}^m) d_{p,i}^k, \quad r_{s,j}^m = \sum_{k=1}^8 N_{p,i}^k(\xi_{s,j}^m, \eta_{s,j}^m) r_{p,i}^k \quad (10)$$

where  $N_p$  is the shape function for an 8-noded shell element, and  $(\xi_{s,j}^m, \eta_{s,j}^m)$  are natural coordinates for the  $m$ -th node of the  $j$ -th beam element within the  $i$ -th plate element as shown in Fig. 4. The symbol  $i$  for the plate element is not shown in Eq. (10).

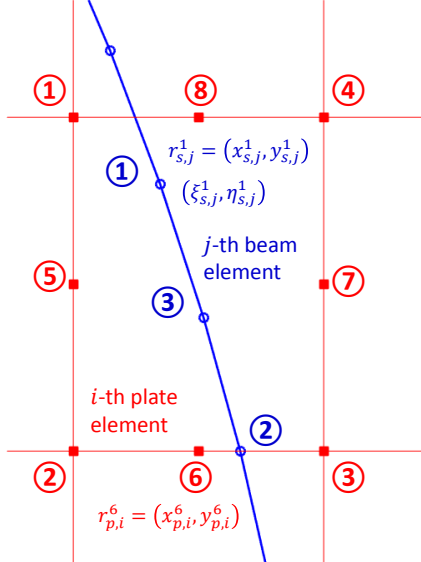


Figure 4: Approximation of stiffener beam element nodal displacement in term of those for the plate element

Based on this method, one can approximate all stiffener beam element nodal displacements and geometry fields using those for the plate. The geometry and displacement fields of the stiffener for the full model can be written in matrix forms as:

$$\mathbf{d}_{sg} = \mathbf{N}_{sp} \mathbf{d}_p, \quad \mathbf{r}_s = \mathbf{N}_{sp} \mathbf{r}_p \quad (11)$$

Note that  $\mathbf{d}_{sg}$  means the stiffener displacement described in the global coordinate system, which can be transformed to that described in the stiffener local coordinate system using

transformation matrix of  $\mathbf{T}_s$ . Also, since all stiffeners are modeled using composite beam elements, and all the beam element nodal displacements are approximated using that for the plate. The displacement compatibility conditions at the stiffener/stiffener interfaces are satisfied automatically.

Mesh examples of a stiffened plate with four arbitrarily shaped stiffeners are shown in Fig. 5 to demonstrate the benefit of the present method. When there is a change in a stiffener's shape, the conventional finite element methods need to re-mesh the structure for finite element analysis in both the plate and all stiffeners as shown in Figs. 5a and 5c. The present method only needs to re-mesh the stiffener where the shape is changed as seen in Figs. 5b and 5d.

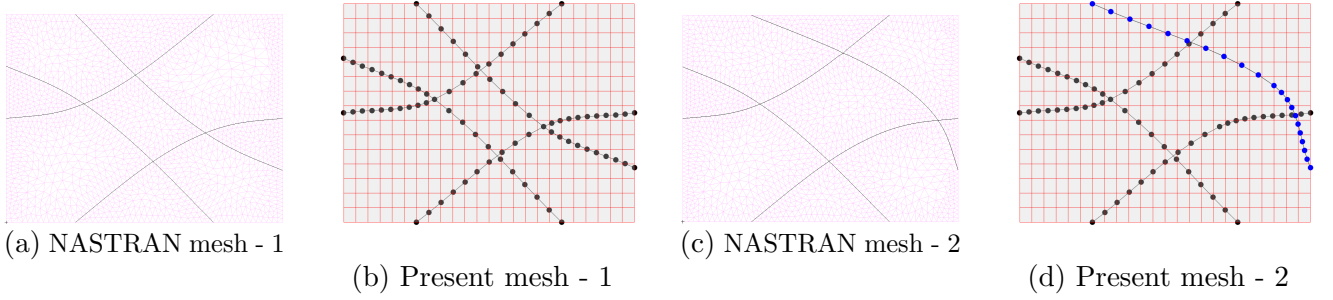


Figure 5: Mesh examples of a stiffened plate with arbitrarily shaped stiffeners

#### D. Finite Element Buckling Analysis

A linear buckling analysis is considered. Thermal effect,  $\Delta T$ , and uniform axial loads,  $\mathbf{F}$ , are considered in the current work. The procedure is to perform a pre-buckling analysis to obtain the stress distribution in both the panel and stiffeners. The geometric stiffness for both the plate and stiffeners is computed in terms of the computed stress distribution. The mechanical strain and thermal expansion used in Eq. (2) are used for computing the stress in the plate. Similarly, the stress in the stiffener is computed using Eq. (6). For a linear static analysis, the stress can be obtained:

$$(\mathbf{K}_p + \mathbf{K}_s) \mathbf{d}_p = \mathbf{F} \quad (12a)$$

$$\boldsymbol{\sigma}_p = \mathbf{Q}_p \mathbf{B}_p \mathbf{d}_p \quad (12b)$$

$$\boldsymbol{\sigma}_t = \mathbf{Q}_s \mathbf{B}_s \mathbf{T}_s \mathbf{N}_{sp} \mathbf{d}_p \quad (12c)$$

Note that the values of  $\mathbf{B}_p$  and  $\mathbf{B}_s$  are different when computed at different Gaussian integration points. In this work, we considered an averaged stress for both the plate and the stiffener using those computed at all Gaussian integration points for the plate and the stiffeners individually [39].

An eigenvalue analysis is conducted for the buckling load factor,  $\lambda$ :

$$[(\mathbf{K}_p + \mathbf{K}_s) + \lambda (\mathbf{K}_{Gp} + \mathbf{K}_{Gs})] \{\mathbf{u}_p\} = \mathbf{0} \quad (13)$$

where  $\mathbf{K}_p$  and  $\mathbf{K}_s$  are the elastic matrices for the panel and the stiffeners, respectively;  $\mathbf{K}_{Gp}$  and  $\mathbf{K}_{Gs}$  are the differential stiffness matrices for the panel and the stiffeners due to the in-plane stresses, respectively;  $\lambda$  is the buckling load factor and the corresponding buckling mode shape is  $\{\mathbf{u}_p\}$ .

The element stiffness matrices,  $\mathbf{K}_p^e$  and  $\mathbf{K}_s^e$ , the element differential stiffness matrices,  $\mathbf{K}_{Gp}^e$  and  $\mathbf{K}_{Gs}^e$  and the element mass matrices, respectively, are:

$$\begin{aligned} \mathbf{K}_p^e &= \int_{-1}^{+1} \int_{-1}^{+1} \mathbf{B}_p^T \mathbf{D}_p(\boldsymbol{\theta})^T \mathbf{B}_p \det \mathbf{J}_p d\xi d\eta, \quad \mathbf{K}_s^e = \int_{-1}^{+1} \mathbf{N}_{sp}^T \mathbf{T}_s^T \mathbf{B}_s^T \mathbf{D}_s^T \mathbf{B}_s \mathbf{T}_s \mathbf{N}_{sp} \det \mathbf{J}_s d\xi \\ \mathbf{K}_{Gp}^e &= \int_{-1}^{+1} \int_{-1}^{+1} (\mathbf{B}_p^{NL})^T \boldsymbol{\sigma}_p \mathbf{B}_p^{NL} \det \mathbf{J}_p d\xi d\eta, \quad \mathbf{K}_{Gs}^e = \int_{-1}^{+1} \mathbf{N}_{sp}^T \mathbf{T}_s^T (\mathbf{B}_s^{NL})^T \boldsymbol{\sigma}_s \mathbf{B}_s^{NL} \mathbf{T}_s \mathbf{N}_{sp} \det \mathbf{J}_s d\xi \end{aligned} \quad (14)$$

where  $\mathbf{J}_p$  and  $\mathbf{J}_s$  are the Jacobians for the panel and the stiffener, respectively, both of which are given in Ref. [20]. The integration required for the stiffness and mass matrices calculations for the composite panel and the composite stiffeners are computed by using Gaussian quadrature rules [40].

### III. Geometry Parameterization for Curvilinear Stiffener

Both straight and curved stiffeners are considered in this work. To generate such curves, Hobby spline [30] is used to parameterize the arbitrarily shaped stiffeners in any physical space. This is because the NURBS curves used in previous works [20, 24] do not pass through all control points, which make it inconvenient to use locations of control points to determine the shape of stiffeners. An additional step is often needed to check whether the parameterized stiffener is located within the plate or not when using NURBS for stiffener shape parameterization. Hobby's spline allows the curve to pass through all control points, which could satisfy the constraints on the locations of parameterized curves in the surface without the need for the additional location check. Additionally, Hobby spline allows local change in the curve without the effect on the global shape while the polynomials change the curve global shape.

The parameterization of an arbitrarily shaped curve lying inside a surface has been studied in previous works by the present authors [20, 24, 41, 42]. Both three- and four-noded NURBS curves are used. Note that the more the number of control points, the more the number of design variables. In this paper, we use three control points to define the shape of an arbitrarily shaped curve. The start and end control points are determined from the placement parameters and the middle point is parameterized using a shape parameter.

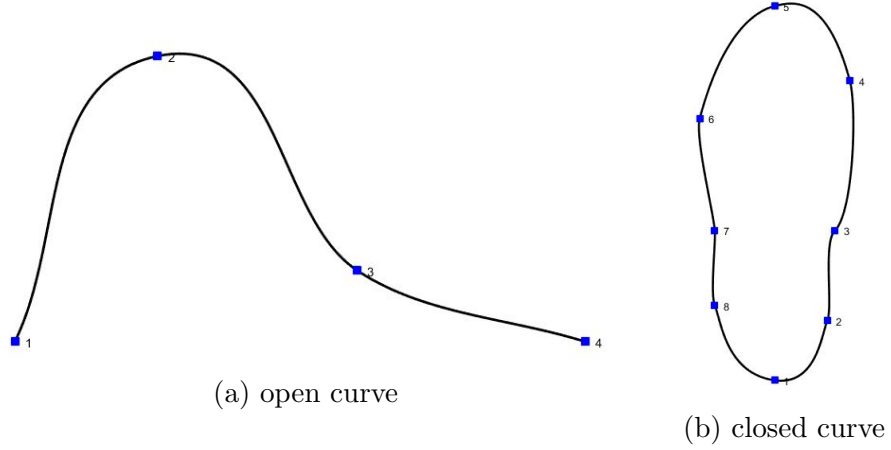


Figure 6: Two examples of Hobby spline [30]

### A. Placement parameter

The parameterization on the placement has been presented in detail in our previous work; however, for completeness, we briefly present the method in this section. To reduce the number of the shape design variables, the start and end points, A and B, are parameterized by a perimeter parameter,  $\epsilon$ , starting from 0 to 1 as shown in Fig. 7. The perimeter parameter for each point, A or B, is then transformed to a natural space which is used in the finite element method. This transformation uses the advantage of the shape functions ( $N_{1,2,3,4}$ ) for a four-noded quadrilateral shell element, so that it works for any shaped quadrilateral plate. The natural coordinates for the start and end points can be obtained from Table 1. One of the four edges could be collapsed, so that the method works for a triangular plate.

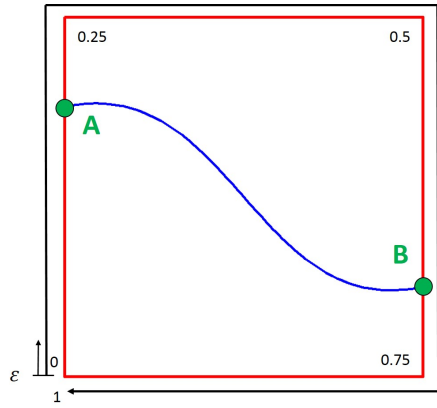


Table 1: The relationship between the perimeter parameter,  $\varepsilon$ , and the natural coordinates,  $\xi$  and  $\eta$

$\varepsilon$	$\xi$	$\eta$
$[0, 0.25]$	-1	$-1+8\varepsilon$
$[0.25, 0.50]$	$-1+8(\varepsilon - 0.25)$	1
$[0.50, 0.75]$	1	$-8(\varepsilon - 0.5) + 1$
$[0.75, 1.00]$	$-1-8(\varepsilon - 1)$	-1

Figure 7: Parameterization of start and end point locations, points A and B

The physical coordinate for start and end points, A and B, in physical space are:

$$\begin{aligned}
x_A &= N_1(\xi_A, \eta_A)x_1 + N_2(\xi_A, \eta_A)x_2 + N_3(\xi_A, \eta_A)x_3 + N_4(\xi_A, \eta_A)x_4 \\
y_A &= N_1(\xi_A, \eta_A)y_1 + N_2(\xi_A, \eta_A)y_2 + N_3(\xi_A, \eta_A)y_3 + N_4(\xi_A, \eta_A)y_4 \\
x_B &= N_1(\xi_B, \eta_B)x_1 + N_2(\xi_B, \eta_B)x_2 + N_3(\xi_B, \eta_B)x_3 + N_4(\xi_B, \eta_B)x_4 \\
y_B &= N_1(\xi_B, \eta_B)y_1 + N_2(\xi_B, \eta_B)y_2 + N_3(\xi_B, \eta_B)y_3 + N_4(\xi_B, \eta_B)y_4
\end{aligned} \tag{15}$$

where  $x_{1,2,3,4}$  and  $y_{1,2,3,4}$  are physical coordinates of the four vertices of a quadrilateral plate. One can refer [43] for more details.

## B. Shape parameter

The shape of an arbitrarily shaped stiffener was parameterized using a distance where the middle control point moves perpendicular to the line between the start and the end points [20, 42]. This moving distance depends on the start and end points locations for defining the middle control point location. It is hard to set the upper and lower bounds for such shape parameters in an optimization study. In this work, we use the natural coordinates,  $\langle\xi, \eta\rangle$ , as shown in Eq. (15) to quantify the location of the middle control point. As long as the constraint of  $-1 \leq \langle\xi, \eta\rangle \leq 1$  is satisfied, the middle control point is located in the panel. One can use Eq. (15) to obtain its physical coordinates,  $(x_C, y_C)$ , in surface using the natural coordinates  $(\xi_C, \eta_C)$ . The physical coordinates for the three control points can be used to generate a curve for the stiffener using Hobby spline.

In summary, for one curve parameterized using the present approach, there are four shape design variables including two perimeter parameters for the start and end points and two natural coordinates for the middle control point. There is still some chance that some parts of the curve generated using Hobby spline are located outside the physical space. Nevertheless, as compared to that using NURBS, the present parameterization approach allows one to have same upper and lower bounds,  $[-1, 1]$ , for all shape parameters. The NURBS curve is located in the polygons generated by the control points, it is possible to have NURBS curve located in the physical space while the middle control point is outside the physical space. This leads a difficulty in defining upper and lower bounds for all shape parameters, when using NURBS for parameterizing curvilinear stiffeners shape, in shape optimization. This difficulty can be overcome when using Hobby spline for parameterizing the curvilinear stiffeners. Additionally, the present method uses area equal method to determine the stiffener element node locations [20, 22]. When one stiffener element node is outside the surface, the area equality constraint is not satisfied, which can be used to quantify the stiffener shape parameter violation in the shape optimization.

## IV. Thermal Buckling of Composite Panel

The section verifies the present program in thermal buckling analysis of composite panel with both straight and curvilinear fibers. Both uniform and nonuniform temperature changes

are studied in this section. Note that the temperature used in the present work represents the temperature change or temperature gradient,  $\Delta T$ ; for convenience, the buckling temperature shown in the following sections represents the buckling temperature gradient.

### A. Uniform Temperature for Composite Panel with Straight Fibers

A simply-supported rectangular composite panel with aspect ratio ( $a/b = 1.25$ ) with dimensions of  $(a \times b \times h) = (15 \times 12 \times 0.048)m$ , the material properties are given in Table 2. Both symmetrically cross-ply and angle-ply laminated panels are studied, in both convergence and verification studies as shown in Table 3. It can be seen that for both cases, the results converge with the plate mesh size. Also, the converged results match well with the results available in literature. Since the shear deformation is considered in the present analysis, the obtained results are slightly lower than the results obtained without including shear deformation.

Table 2: Material properties of composite material

$E_L$ (MPa)	$E_T$ (MPa)	$G_{LT}$ (MPa)	$\nu_{12}$	Layer thickness (m)	$\alpha_1$ ( $^{\circ}\text{C}^{-1}$ )	$\alpha_2$ ( $^{\circ}\text{C}^{-1}$ )
22.5	1.17	0.66	0.22	$6 \times 10^{-3}$	$-0.04 \times 10^{-6}$	$16.7 \times 10^{-6}$

Table 3: Convergence and verification studies on thermal buckling of a composite panel under a uniform temperature

Mesh size	$[0/90/90/0]_s$	$[0/45/-45/90]_s$
$8 \times 6$	12.23	13.62
$12 \times 8$	12.24	13.64
$18 \times 12$	12.25	13.65
$24 \times 18$	12.25	13.65
$32 \times 24$	12.25	13.65
Shi <i>et al.</i> [44]	12.26	13.71
Shiau <i>et al.</i> [10]	12.26	13.75
Ounis <i>et al.</i> [11]	12.26	13.74

### B. Non-Uniform Temperature for Composite Panel with Straight Fibers

A simply-supported rectangular composite panel with length and width denoted as  $a$  and  $b$ , respectively, used by Meyers and Hyer [45] is employed here to verify the current program in

thermal buckling analysis under nonuniform temperature change. The material properties for this model are given in Table 4. The temperature change  $\Delta T$  is given by,

$$\Delta T = \lambda_T \left( 1 + \bar{T} \frac{z}{H} \right) \quad (16)$$

where  $\lambda_T$  is the factor for the temperature change at the midplane of the plate,  $H$  is the total panel thickness,  $z$  is the thickness coordinate, and  $\bar{T}$  controls the magnitude of the through-the-thickness gradient. When the value of  $\bar{T}$  is positive, it means the top side is warmer than the bottom side. In this verification study case,  $\bar{T} = 0.05$ .

Table 4: Material properties of composite material

$E_1$ (GPa)	$E_2$ (GPa)	$G_{12}$ (GPa)	$\nu_{12}$	Layer thickness (m)	$\alpha_1$ ( $^{\circ}\text{C}^{-1}$ )	$\alpha_2$ ( $^{\circ}\text{C}^{-1}$ )
155.00	8.07	4.55	0.22	$1.272 \times 10^{-4}$	$-0.07 \times 10^{-6}$	$30.1 \times 10^{-6}$

Mesh convergence study on thermal buckling load for the quasi-isotropic square composite panel subjected to a nonuniform temperature change was conducted as shown in Table 5. It is seen that the results change slightly with the mesh size. The converged result using mesh size of  $18 \times 18$  for the panel matches well with the reference result. As expected, the result with shear deformation considered in the plate's motion is slightly lower than the result available in the literature.

Table 5: Convergence and verification studies on buckling temperature of a square composite panel,  $a = b = 0.15$  m, quasi-isotropic laminate configuration  $[\pm 45/0/90]_s$

Mesh size	$8 \times 8$	$12 \times 12$	$18 \times 18$	$24 \times 24$	$36 \times 36$	Meyers and Hyer [9]
Buckling temperature, $^{\circ}\text{C}$	38.54	38.53	38.52	38.51	38.51	38.6

Considering the possible skew angle of the material axes relative to the edge of the plate [9], a parametric study on the buckling temperature in terms of various skew angles is conducted. The skew angle is defined by rotating all fiber plies about the  $z$ -axis by one angle,  $\alpha$ , in a counter-clockwise direction. If the skew angle is  $\alpha = 30$  degrees, for example, then the  $[\pm 45/0_2]_s$  laminates become the fiber ply orientations of  $[+75/-15/30_2]_s$ .

The mesh size for the plate is  $18 \times 18$ . Two different plate aspect ratios for the plate,  $a/b = 1$  and  $a/b = 2$ , are studied with a fixed width,  $b = 0.15$  m. Figure 8 shows the predicted results match very well with the results available in literature [9] where  $\Delta T^* = 38.52$   $^{\circ}\text{C}$  is buckling temperature for the square quasi-isotropic composite panel with zero skew angle. It is observed from Fig. 8 that the square panel has a larger buckling temperature than that of the rectangular panel. The skew angle decreases the buckling temperature for the square panel ( $a/b = 1$ ) by more than 20% while the positive skew angle leads to a  $\sim 10\%$  increase

in the buckling temperature for the rectangular panel ( $a/b = 2$ ) at the studied skew angle range up to 30 degrees.

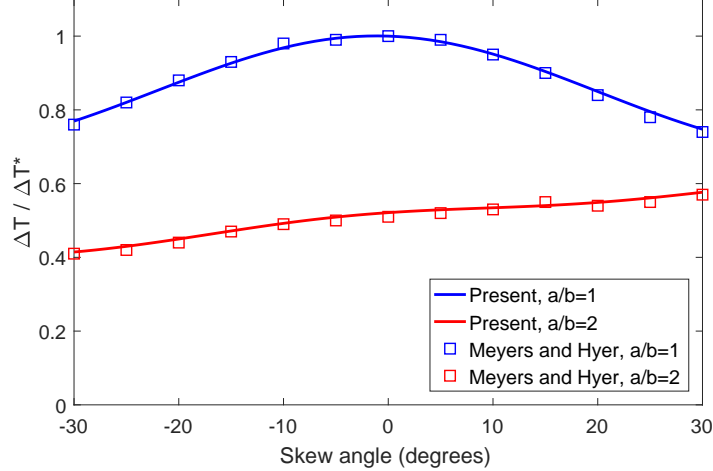


Figure 8: Buckling temperature with skew angle,  $\alpha$

### C. Uniform Temperature for VAT Laminated Panel

In this case, a uniform temperature change is considered for a simply-supported VAT laminated panel studied by Duran et al. [14] to verify the present program on thermal buckling analysis on VAT laminated plates. A square composite panel with side length of  $a = 0.15\text{m}$  and the thickness of  $h = 1.016\text{mm}$  is considered. A four-layer symmetric laminate configuration ( $\pm\langle\theta_0|\theta_1\rangle_s$ ) is used. Different materials for the VAT laminates are studied whose properties can be found in Table 6.

Table 6: Material properties

Case	Material	$E_1$ (GPa)	$E_2$ (GPa)	$G_{12}$ (GPa)	$\mu_{12}$	$\alpha_1$ ( $1/\text{ }^\circ\text{C}$ ) $10^{-6}$	$\alpha_2$ ( $1/\text{ }^\circ\text{C}$ ) $10^{-6}$
(a)	Graphite/Epoxy	155	8.07	4.55	0.22	-0.07	30.1
(b)	E-Glass/Epoxy	41.	10.04	4.3	0.28	7.0	26.
(c)	S-Glass/Epoxy	45.	11.0	4.5	0.29	7.1	30.
(d)	Kevlar/Epoxy	80.	5.5	2.2	0.34	-2.0	60
(e)	Carbon/Epoxy	147.	10.3	7.0	0.27	-0.9	27
(f)	Carbon/PEEK	138	8.7	5.0	0.28	-0.2	24
(g)	Carbon/Polyimide	216	5.0	4.5	0.25	0.0	25
(h)	Boron/Epoxy	201.	21.7	5.4	0.17	6.1	30.

The present results in thermal buckling temperature for all material cases agree very well

with those obtained by Duran et al. [14] as shown in Table 7. Both NASTRAN and ABAQUS are also used to compute the thermal buckling temperatures as shown in Table 7. It is found that the present buckling temperatures agree well with NASTRAN and ABAQUS results for all cases except for Cases (d) and (e); large differences in the buckling temperature for these two cases are observed. The buckling mode shapes for all cases compare well among the three results as shown in Figs. 11 and 12 while there are some differences for mode shapes for Cases (d) and (e). Previous works [22, 39] have found that the buckling loads for the VAT laminates under in-plane mechanical loads computed using the present program agree well with NASTRAN results. Note that the in-plane stress resultants studied in this work are generated under restrained thermal expansion. Considering ABAQUS results are same as NASTRAN results, we use NASTRAN to study the thermal stress distribution.

Table 7: Comparisons of buckling temperature for square VAT laminated panel with different materials,  $(\pm \langle \theta_0 | \theta_1 \rangle)_s$

Case	Material	$\langle \theta_0   \theta_1 \rangle$ (degrees)	$\Delta T_{crit}$ (°C) (Duran <i>et al.</i> [14])	Present (°C)	Diff.	NASTRAN °C (Diff.)	ABAQUS °C (Diff.)
(a)	Graphite/Epoxy	$\langle 60.70   32.19 \rangle$	34.26	33.70	-1.64%	32.68 (3.1%)	31.91 (5.6%)
(b)	E-Glass/Epoxy	$\langle 6.71   58.04 \rangle$	5.58	5.52	-1.08%	5.54 (-0.4%)	5.47 (0.9%)
(c)	S-Glass/Epoxy	$\langle 16.12   54.74 \rangle$	5.04	4.99	-1.05%	5.02 (-0.6%)	4.96 (0.6%)
(d)	Kevlar/Epoxy	$\langle 66.05   11.73 \rangle$	22.18	21.93	-1.15%	16.27 (34.8%)	16.06 (36.5%)
(e)	Carbon/Epoxy	$\langle 69.00   -5.705 \rangle$	57.79	57.24	-0.96%	34.02 (68.3%)	33.76 (69.6%)
(f)	Carbon/Peek	$\langle 63.07   29.50 \rangle$	38.08	37.55	-1.38%	35.55 (5.6%)	34.85 (7.8%)
(g)	Carbon/Polyimide	$\langle 56.30   36.68 \rangle$	78.28	76.65	-2.08%	76.94 (-0.4%)	74.61 (2.7%)
(h)	Boron/Epoxy	$\langle -6.57   63.28 \rangle$	7.50	7.34	-2.08%	7.53 (-2.5%)	7.32 (0.3%)

The first-layer thermal stress along the material principal 1–axis,  $\sigma_1$ , computed using NASTRAN and the present method are compared as shown in Fig. 9. For a uniform temperature change, the thermal stress,  $\sigma_1$ , for all elements for each layer described in the material coordinate system computed using the present method are same as expected while they are not same in NASTRAN results. For Kevlar/Epoxy case, there are larger differences in stress in all elements, which result in a large difference in the buckling temperature between the present and the NASTRAN results. For the S-Glass/Epoxy material, the principal stress,  $\sigma_1$ , for all elements are also not same but the magnitudes for stresses for all elements are close. It is observed that the magnitude of thermal expansion coefficient,  $\alpha_1$ , for Cases (d) and (e) larger than others. Taking Case (d) for an example, when changing the value of  $\alpha_1$  from negative to positive, the thermal buckling temperature obtained from NASTRAN and the present method become close as shown in Fig. 10. This shows that for a VAT laminated structure, both NASTRAN and ABAQUS may have a deficiency in computing thermal buckling temperature when the material has both positive and negative thermal expansion coefficients.

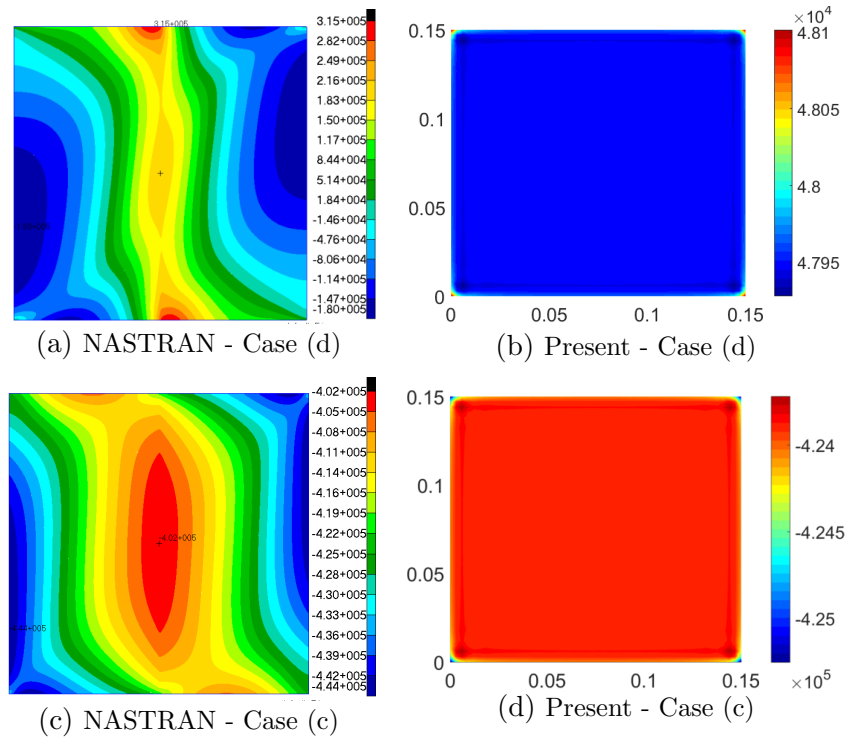


Figure 9: First-layer stress along material principal direction,  $\sigma_1$  at a unit temperature change,  $\Delta T = 1^\circ\text{C}$

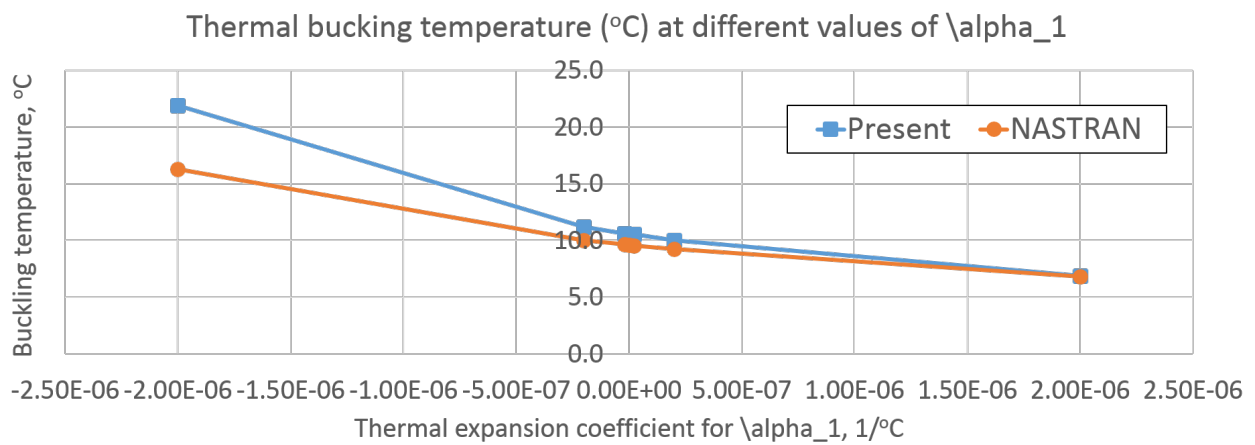


Figure 10: Buckling temperature changes with thermal expansion coefficient,  $\alpha_1$ , for Case (d)

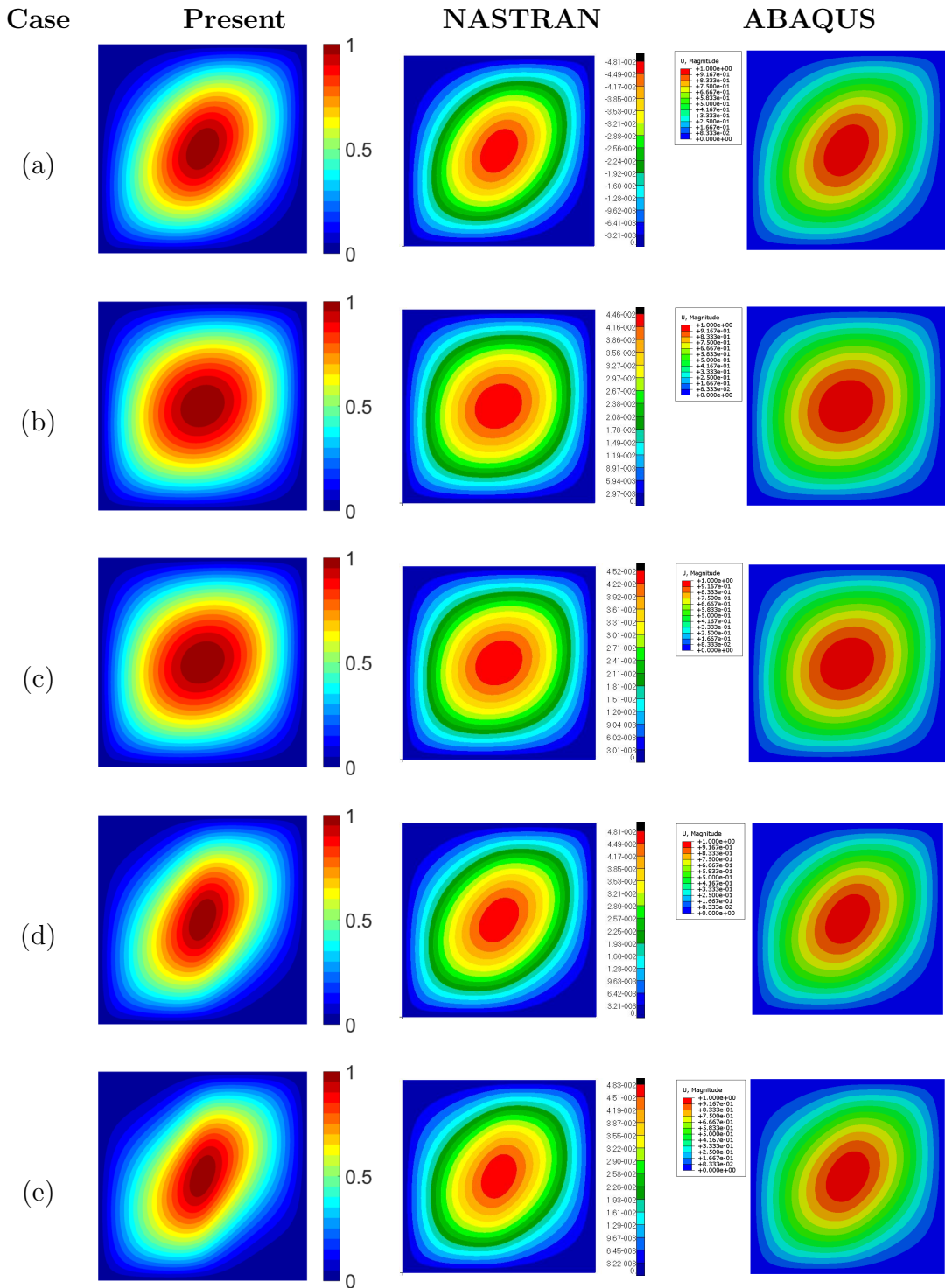


Figure 11: Thermal buckling mode shape for different material cases (Con't)

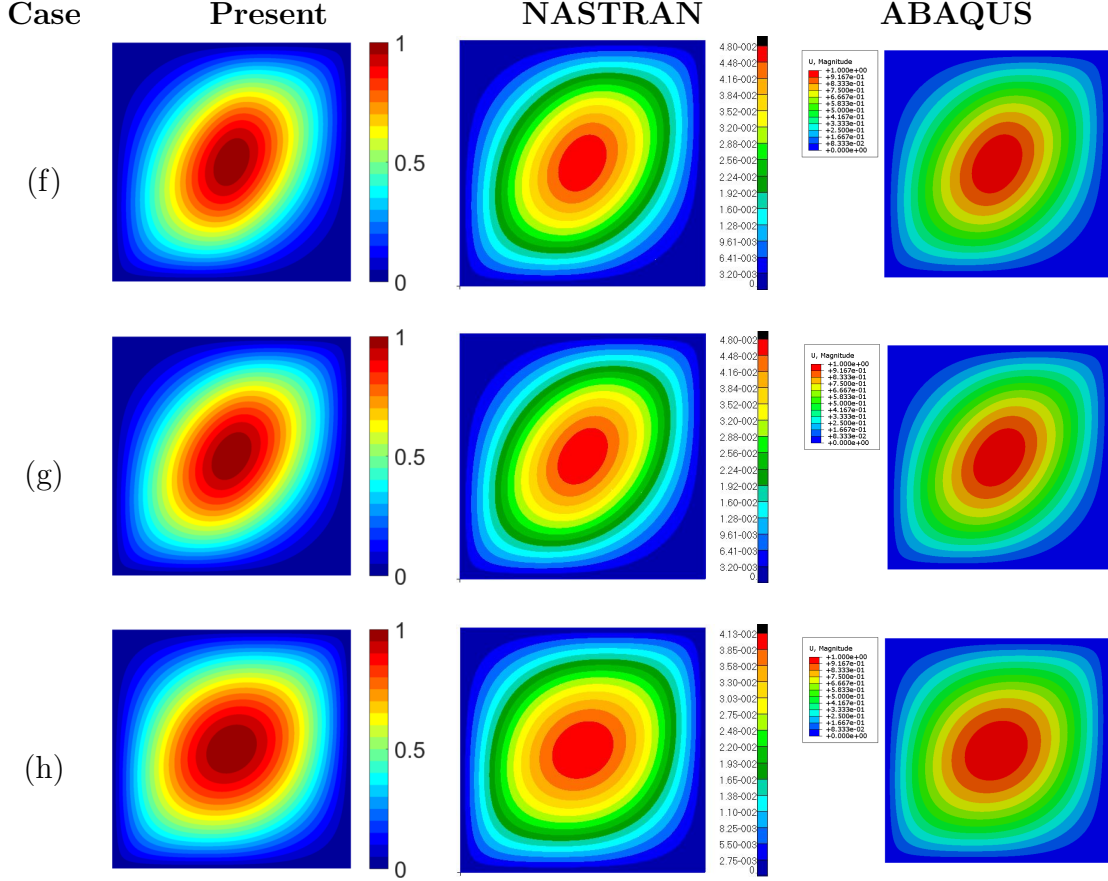


Figure 12: Thermal buckling mode shape for different material cases

## V. Thermal Buckling of Curvilinearly Stiffened Plate

Previous study by Zhao and Kapuria [20] has verified the present program on the buckling of a stiffened plate with both straight and curvilinear stiffeners. Additionally, Section IV has verified the present program in studying the thermal buckling of unstiffened composite plate under both uniform and nonuniform temperature change using straight-fiber laminates and unstiffened VAT laminates under a uniform temperature change. This section first verifies the present program for studying the thermal buckling of a curvilinearly stiffened composite plate under a uniform temperature change. After that, parametric studies on the thermal buckling temperature, in terms of (a) the VAT laminates for a stiffened plate with two straight stiffeners and (b) curvilinear stiffener shape for a curvilinearly stiffened VAT laminated plate, are presented. Finally, an optimization study is conducted for a curvilinearly stiffened VAT laminates in terms of both VAT laminates and stiffener shape for maximizing the thermal buckling temperature.

## A. Verification Study

A simply-supported rectangular composite plate studied in the previous work [22] is used for verifying the thermal buckling of a curvilinearly stiffened laminated plate subjected to a uniform temperature,  $\Delta T$ . The physical coordinates for the curve ① are given in Appendix A. The second curve ② is antisymmetric about the diagonal line of the rectangular plate,  $y = \frac{b}{a}x$ . The geometric dimensions for both the plate and the stiffeners are described in Fig. 13. An eight-layer antisymmetric laminates with straight-fibers for each layer are considered for the plate with laminate configurations of  $[(\pm 45)_2]_{AS}$ . The stiffeners are modeled as orthotropic beams whose material properties are same as that for the plate and can be found in Ref. [22].

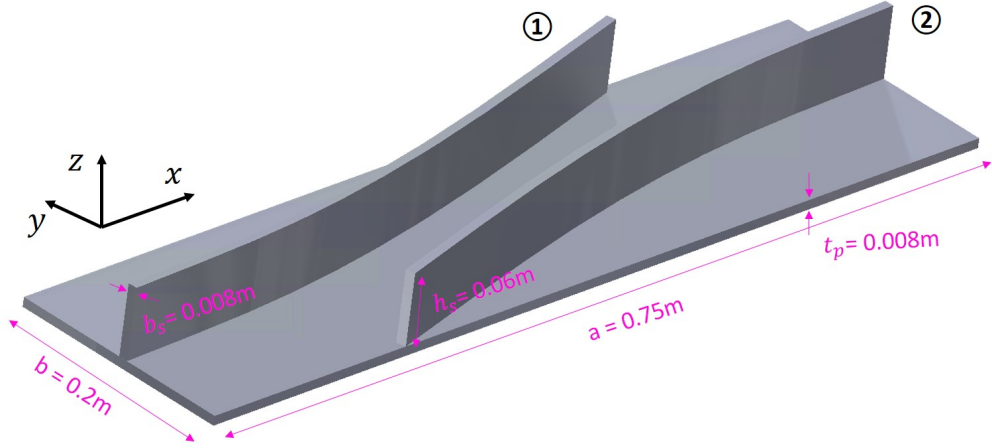


Figure 13: Stiffened composite plate with two curvilinear stiffeners

Since there is no available result regarding thermal buckling of curvilinearly stiffened composite plates, NASTRAN results are used to verify the present program for thermal buckling analysis. Both concentric and eccentric stiffeners are considered. Note that this work is not to compare the computing efficiency of the two methods but to verify the present program using the NASTRAN results. To get a converged result for a subsequent comparison, a relatively fine mesh is considered for the NASTRAN model with 4892 triangular elements (CTRIA3) for the plate and 100 beam elements (CBEAM) for each stiffener. Note that the glue contact cannot be used for the stiffened plate when there exist offsets in the beam models and the plate elements when using NASTRAN because the eccentric stiffeners are modeled as beam elements in the present work. Another reason of using a relatively fine mesh for the curvilinearly stiffened plate in NASTRAN is that the fine mesh is often used to avoid a meshing failure, as observed in previously developed aircraft wing design using EBF3GLWingOpt [46]. The convergence and verification studies regarding the thermal buckling for the unstiffened plate are conducted first. However, for brevity, they are not shown here as Section IV already presents the results for thermal buckling of the unstiffened

plate, in detail. A converged mesh for the plate of  $30 \times 20$  is considered in the present analysis. Figure 14 shows the NASTRAN mesh and the present mesh for the curvilinearly stiffened plate.

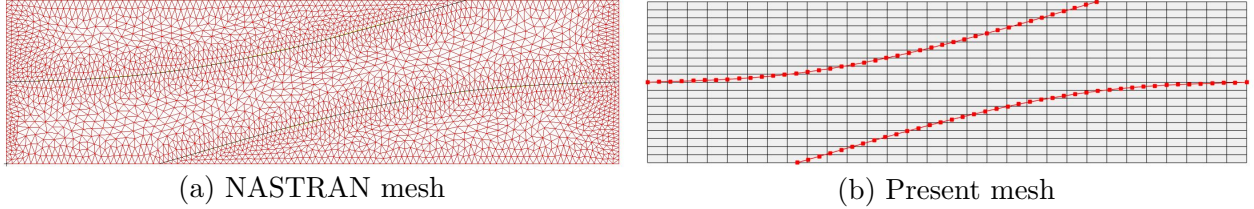


Figure 14: Finite element models used in NASTRAN and present program

Table 8: Mesh convergence and verification studies of buckling temperature of stiffened laminated plate with each stiffener beam elements number, fixed plate mesh size:  $30 \times 20$  (Unit:  $^{\circ}\text{C}$ )

Mode	Concentric stiffeners					Eccentric stiffeners					
	No.	5	10	20	40	NASTRAN	5	10	20	40	NASTRAN
1	1059.3	1072.6	1079.4	1079.6	1083.8 (-0.41%)		1482.2	1541.2	1569.0	1584.6	1570.4 (-0.09%)
2	2307.8	2357.7	2376.7	2378.2	2361.8 (0.63%)		2653.9	2694.8	2705.9	2708.5	2729.0 (-0.85%)
3	2567.3	2608.3	2624.5	2626.5	2618.8 (0.22%)		2854.8	2992.6	3035.4	3049.8	3054.9 (-0.64%)
4	2816.5	2854.6	2869.3	2871.5	2845.7 (0.83%)		2946.2	3019.5	3069.4	3109.3	3102.7 (-1.07%)
5	3621.1	3694.1	3724.0	3726.8	3699.2 (0.67%)		3802.7	3892.3	3930.6	3962.1	3933.4 (-0.07%)

Table 8 shows the convergence and verification studies of the buckling temperature for the curvilinear stiffened plate with the stiffener beam-element number. For buckling analysis, we are often interested in only the first buckling mode. In the verification studies, for both stiffener cases, the eigenvalues for the first 5 buckling modes are examined. It is observed that there is a less than 1% change in the eigenvalue when doubling the stiffener beam-element number from 20 to 40 for each stiffener. The buckling eigenvalues for both cases are found to converge with the stiffener beam-element number. The thermal buckling temperatures for both cases are computed using 20 beam elements for each stiffener and both results are found in good agreements with NASTRAN results. The mode shapes for the first two buckling modes obtained from the present analysis are compared with the NASTRAN results and a good agreement is observed for buckling mode shapes as shown in Figs. 15 and 16.

Based on this verification work, along with the verification works in Section IV regarding the thermal buckling of unstiffened VAT laminates, it can be concluded that the present program can predict the thermal buckling for the curvilinearly stiffened VAT composite plate under a uniform temperature change.

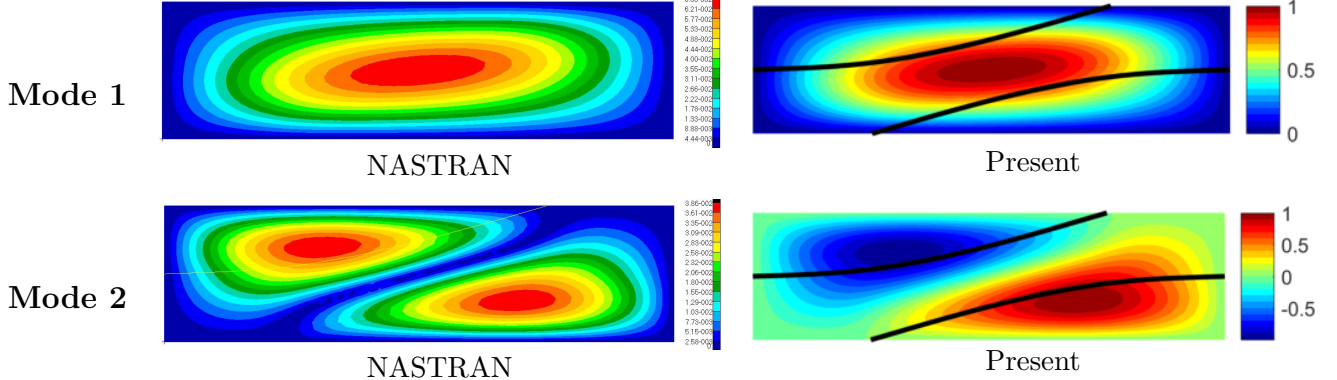


Figure 15: First two thermal buckling mode shapes of a curvilinearly stiffened plate with concentric stiffeners

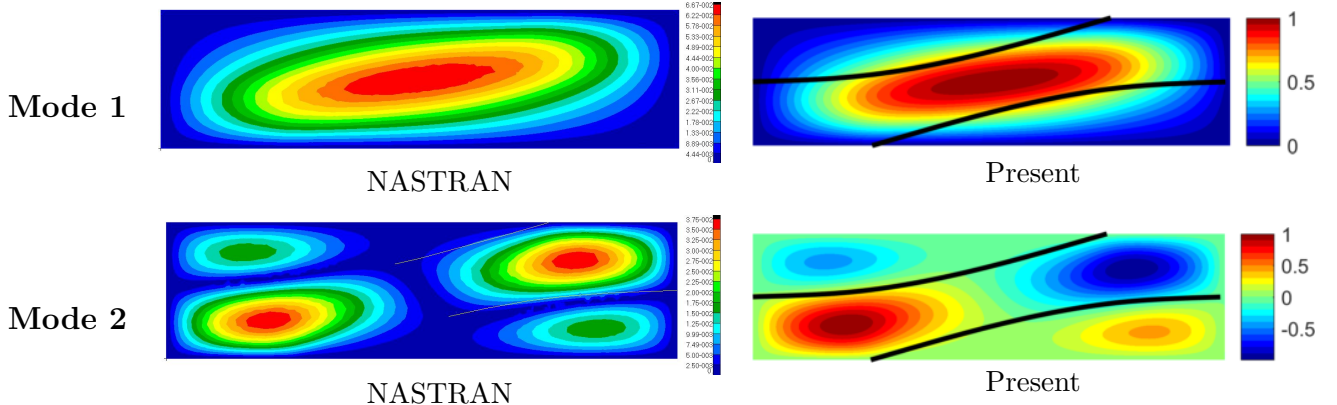


Figure 16: First two thermal buckling mode shapes of a curvilinearly stiffened plate with eccentric stiffeners

## B. Straight Stiffeners

The model studied in Section IV-C along with the composite material, Carbon/Epoxy (seen Table 9 for material properties), used by Duran *et al.* [14], are considered in this section. Two straight equidistant stiffeners [47] placed along the panel width direction, i.e.  $y = b/3$  and  $y = 2b/3$ , are considered as shown in Fig. 17 to study the buckling for stiffened VAT laminates under a uniform temperature change,  $\Delta T$ . The square composite panel has a 8-layer laminate configuration of  $(\pm[\langle\Theta_0|\Theta_1\rangle_2])_S$ . It should be pointed out that the layer thickness given in Ref. [14] doubles the normal thickness given in Table 9. Therefore, in

this paper, we consider the laminates fiber orientations defined as  $(\pm[\langle\Theta_0|\Theta_1\rangle_2])_S$ . A linear fiber ply orientation for the VAT laminates is given as shown in Eq. (1). The material properties for both the laminated plate and the orthotropic stiffeners are same as shown in Table 9. The stiffener depth ratio is fixed as  $h_s/b_s = 5$  and the stiffener width,  $b_s$ , equals the panel thickness. Simply-supported boundary conditions are considered for the studied model where the three displacements,  $u$ ,  $v$  and  $w$ , are zero at the panel's four edges.

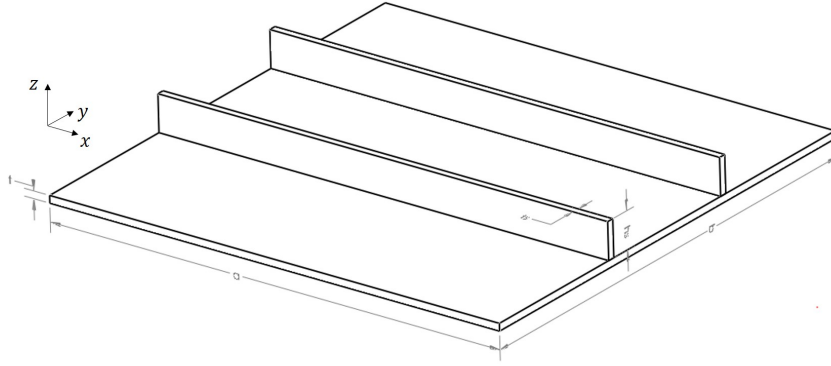


Figure 17: Stiffened plate with two straight stiffeners

Table 9: Material properties of composite material

$E_1$ (GPa)	$E_2$ (GPa)	$G_{12}$ (GPa)	$\nu_{12}$	Layer thickness (m)	$\alpha_1(1/\text{ }^\circ\text{C})$	$\alpha_2(1/\text{ }^\circ\text{C})$
147.00	10.30	7.00	0.27	$1.27 \times 10^{-4}$	$-0.9 \times 10^{-6}$	$27 \times 10^{-6}$

Buckling temperature with the fiber ply orientations for the unstiffened plate, the stiffened plate with two concentric stiffeners and two eccentric stiffeners are shown in Fig. 18. The diagonal line means the buckling temperature for the straight-fiber laminates. It is clearly observed that VAT laminates can improve the buckling temperature for all cases. The maximum buckling temperature and its corresponding optimal laminates are shown in Table 10. The VAT laminates can increase the buckling temperature by up to 97%. As expected, a significant increase in the total buckling temperature can be obtained by adding stiffeners. The buckling mode shapes corresponding to the maximum buckling temperature for each case are shown in Fig. 19.

For optimal straight-fiber laminate configurations as shown in Fig. 19a, the buckling wavelength for the plate is modified when adding two concentric straight stiffeners. Nevertheless, the buckling mode shapes for the three optimal straight-fiber laminate configurations are similar while there is a slight change in the mode shape for the plate with eccentric stiffeners.

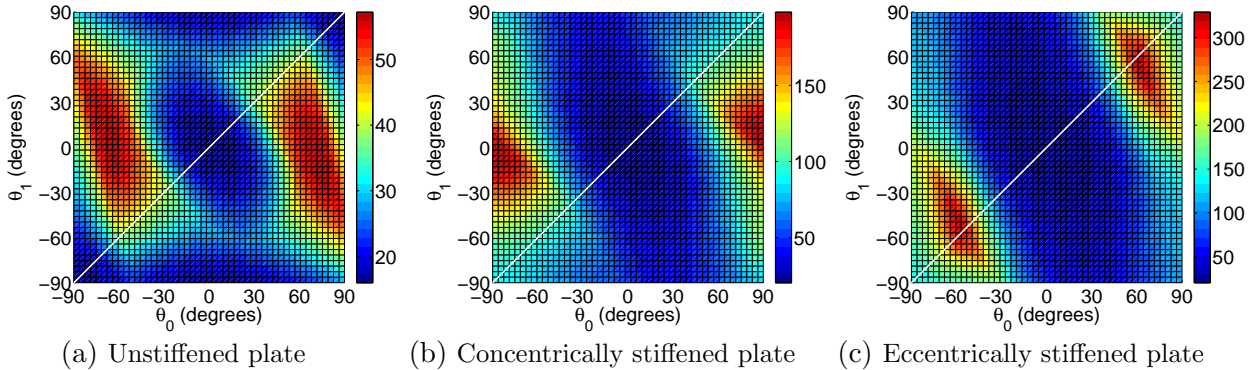


Figure 18: Thermal buckling of unstiffened and stiffened VAT plates under uniform temperature change in terms of VAT laminates fiber ply orientation

Table 10: Maximum buckling temperature,  $\Delta T_{cr}$ , for a square VAT laminated panel

Composites	unstiffened plate	stiffened plate	
		concentric stiffener	eccentric stiffener
SF laminates	41.58 ( $\pm\langle 45.92^\circ   45.92^\circ \rangle$ )	100.4, ( $\pm\langle 49.59^\circ   49.59^\circ \rangle$ )	315.4, ( $\pm\langle 56.94^\circ   56.94^\circ \rangle$ )
VAT laminates	57.24 ( $\pm\langle 69.00^\circ   -5.70^\circ \rangle$ )	198.1, ( $\pm\langle 86.33^\circ   5.51^\circ \rangle$ )	329.2, ( $\pm\langle 60.61^\circ   53.27^\circ \rangle$ )
Improvement	37.66%	97.31%	4.38%

SF: straight-fiber

For the optimal VAT laminate configurations as shown in Fig. 19b, it is found that the optimal buckling mode shapes are completely different for the three laminate configurations. This shows that for a stiffened plate, the VAT laminates can tailor the buckling mode shape in addition to redistributing the in-plane stress resultants for improving the buckling responses. Recall that the curvilinear stiffeners can be used to tailor the buckling mode shape to increase the buckling load [48], it is possible to combine the use of curvilinear stiffeners and VAT laminates to improve the buckling response of a stiffened composite plate.

### C. Curvilinear Stiffeners

For curvilinear stiffener parameterized using the approach as presented in Section III, each stiffener has 4 shape design variables, along with two design variables for the fiber ply orientations, there are a total of 10 design variables for the stiffened plate with two stiffeners. It is very expensive to conduct a complete parametric study with respect to these 10 design variables. An optimization study is conducted to determine the optimal design in the stiffener shape and the laminate configuration. Before the optimization study, a simple parametric study is first conducted to investigate the influence of the stiffener shape on the buckling

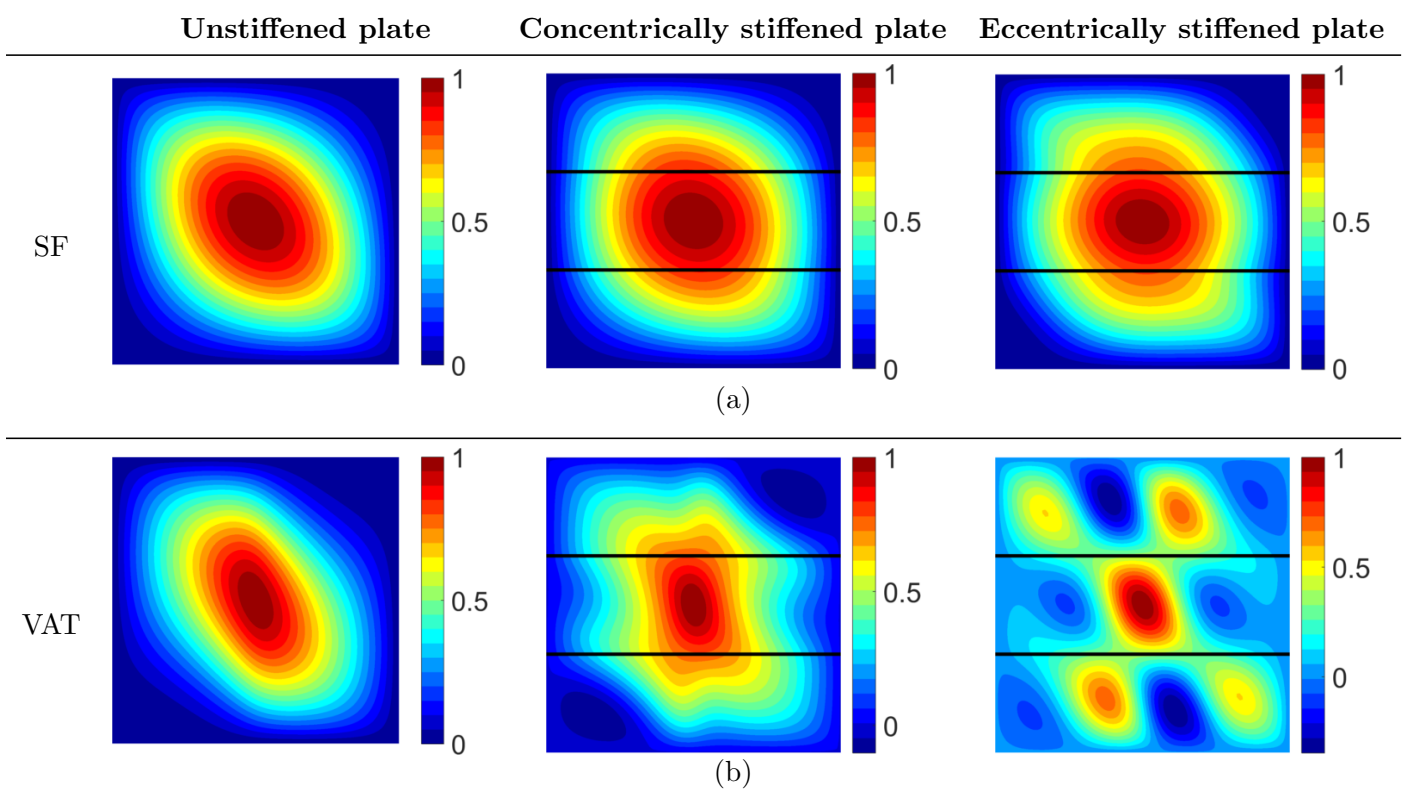


Figure 19: Buckling mode shapes corresponding to the maximum buckling temperature change

temperature of the plate. In fact, there are many stiffeners used for the plate to improve the buckling responses. Considering that the scope of the present paper is to study the effect of both curvilinear stiffener and curvilinear fiber ply orientation on the buckling response, we only employ two curvilinear stiffeners in the parametric and optimization studies to reduce the computational burden in both CPU time and memory size. Also, the size design variables, such as the geometric dimensions in the stiffener cross section, are not considered.

### 1. Simple parametric study

The start and end points for each curve are fixed as shown in Fig. 20. The middle control points for the two stiffeners have natural coordinates of  $(0, \xi_2)$  and  $(0, -\xi_2)$ , respectively. The buckling temperature is studied by varying the parameter of  $\xi_2$  from -1 to 1. The start and end perimeter parameters for the curve ① are  $\varepsilon_1^A = 0.1875$  and  $\varepsilon_1^B = 0.6875$ , respectively. The curve ② is symmetric to the curve ① about the panel center line,  $y = b/2$ . Concentric stiffeners are used and the optimal VAT laminates of  $\langle 86.33^\circ | 5.51^\circ \rangle$  is considered for the plate.

Figure 21 shows the buckling temperature and total weight with the shape parameter,  $\xi_2$ , in the presence of a uniform temperature gradient. As compared to the buckling responses for the plate with straight stiffeners, it is clearly observed that curvilinear stiffeners can improve

the buckling temperature by up to 63.4% with a weight penalty of mere 0.2%  $W_s$  where  $W_s$  is the total structural weight for plate with two straight  $x$ -axis stiffeners. The buckling temperature is found to change with the shape parameter in a discontinuous way. This is because the buckling mode shape changes with the shape parameter as seen in Fig. 22. It is clearly seen that the curvilinear stiffeners change the mode shape by modifying the buckling mode wavelength for improving the thermal buckling response. By comparing the buckling mode shapes for the stiffened plate with the straight stiffeners case,  $\xi_2 = 0.50$ , and the optimal curvilinear stiffeners case,  $\xi = 0.25$ , the buckling mode peaks are moved to the plate's edges using curvilinear stiffeners as shown in Fig. 22, for improving its buckling response. This demonstrates that curvilinear stiffeners can be used to tailor the buckling mode shape to increase the buckling temperature.

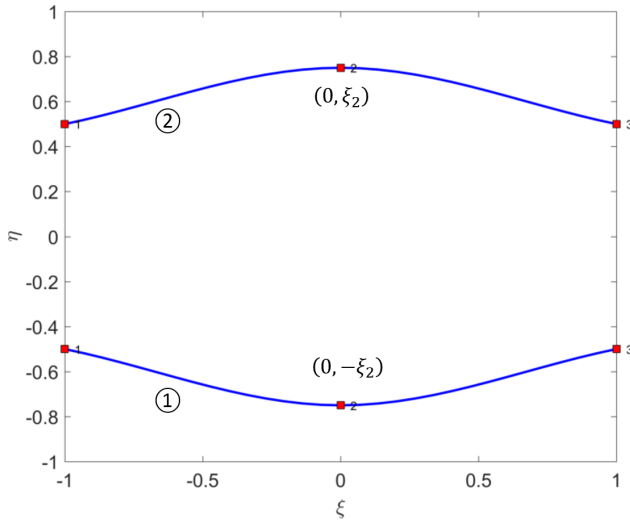


Figure 20: Shape parameter for an arbitrarily shaped stiffener in the natural space

## 2. Buckling optimization results

Previously developed parallel particle swarm optimization (PSO) code [42, 46] is used as the optimizer to maximize the buckling temperature for the stiffened plate with both curvilinear stiffeners and VAT laminates. We consider two cases in the optimization study: (a) buckling temperature maximization using the straight-fiber laminates for the plate, and (b) buckling temperature maximization using VAT laminates for the plate. For both the cases, a maximum weight constraint is considered where the upper bound of the weight is that for the plate with two straight  $x$ -axis stiffeners,  $W_s$ . Arbitrarily shaped stiffeners are considered in both cases. The optimization problem is summarized as:

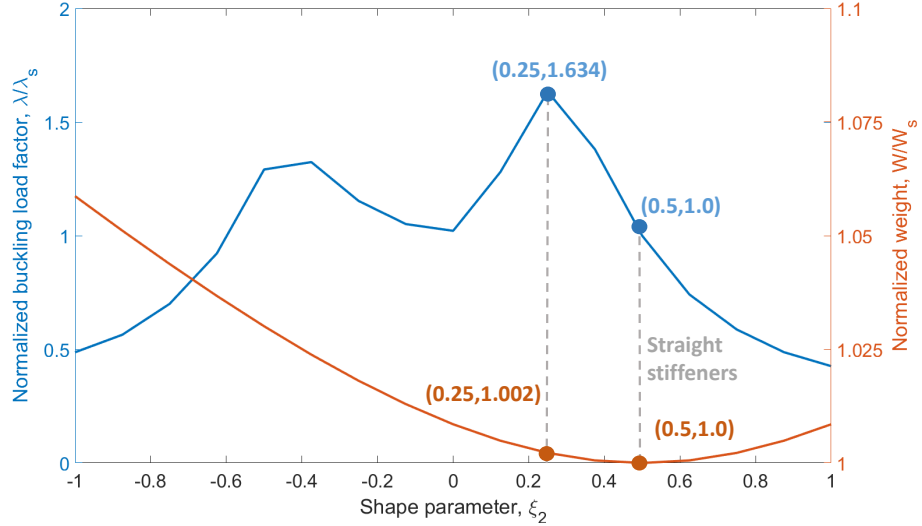


Figure 21: Buckling temperature change with a shape parameter for a curvilinearly stiffened VAT laminated plate

$$\begin{aligned}
 & \text{maximize} && \Delta T_{cr} \\
 & \text{w.r.t.} && \{\Theta_0, \Theta_1, \varepsilon_{1,2}^A, \varepsilon_{1,2}^B, \xi_{1,2}^C, \eta_{1,2}^C\} \\
 & \text{s.t.} && W \leq W_s \\
 & && -90^\circ \leq \{\Theta_0, \Theta_1\} \leq 90^\circ \\
 & && 0 \leq \{\varepsilon_{1,2}^A, \varepsilon_{1,2}^B\} \leq 1 \\
 & && -1 \leq \{\xi_{1,2}^C, \eta_{1,2}^C\} \leq 1
 \end{aligned}$$

The iteration history of the buckling load is shown in Fig. 23. The maximum buckling temperatures for the two cases and their corresponding stiffener shape and the laminate configurations are shown in Table 11. For both cases, the weight constraint is active. A larger buckling temperature change is obtained for the curvilinearly stiffened plate with the VAT laminates for the plate. A 22.14% increase in the buckling temperature is obtained by using VAT laminates and arbitrarily shaped stiffeners as compared to that using straight-fiber laminates and curvilinear stiffeners. The optimal laminate configuration and the stiffener shape for each case are shown in Fig. 24. It is clearly seen that the buckling mode wavelength is modified for improving the buckling temperature for both the cases.

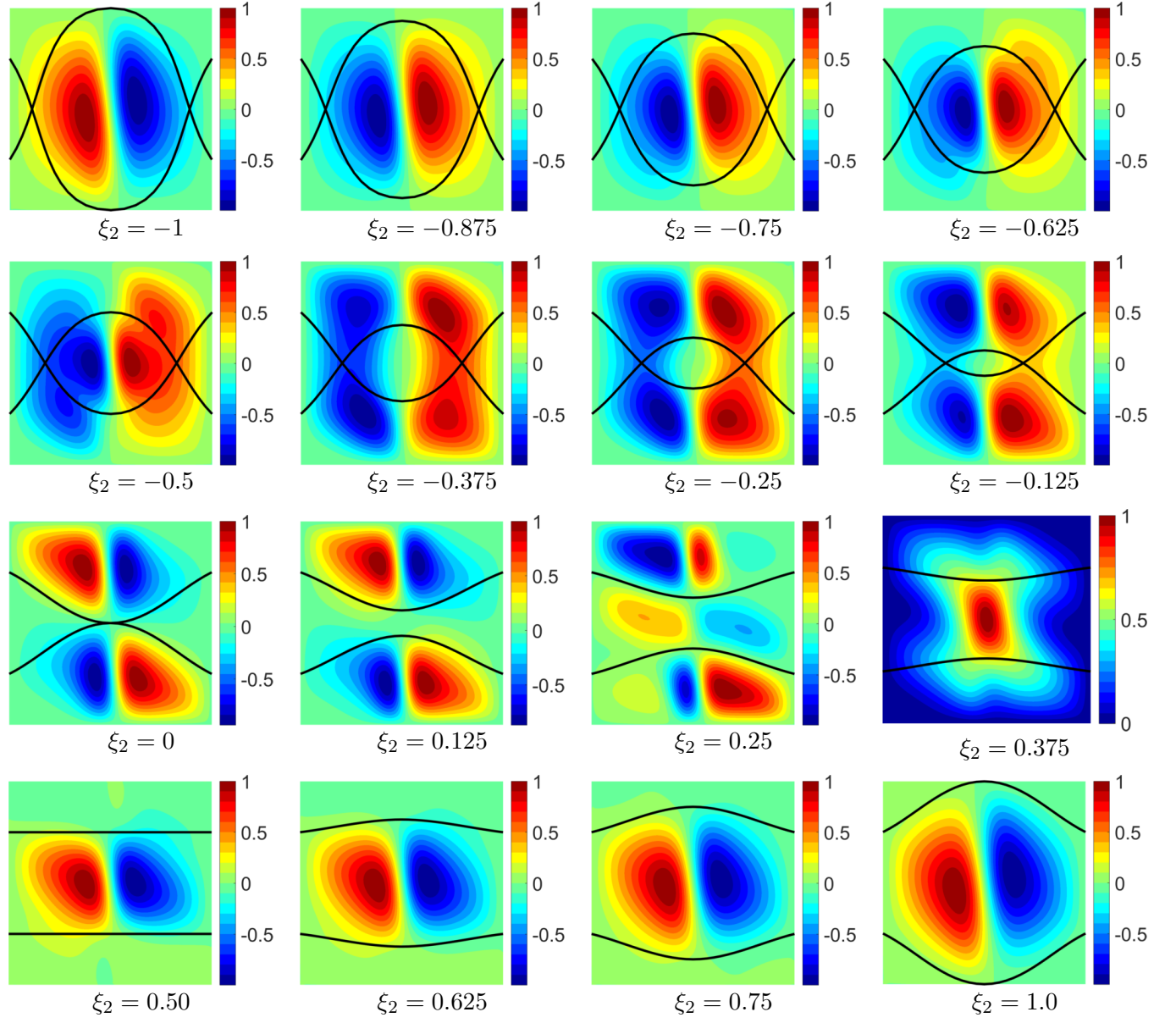


Figure 22: Thermal buckling mode shape for a stiffened plate with different shape parameters,  $\xi_2$

Table 11: Optimal design for the maximum buckling temperature change

Composites	Straight-fiber laminates	VAT laminates
Fiber ply orientation	$\langle 37.72^\circ   37.72^\circ \rangle$	$\langle 64.93^\circ   31.58^\circ \rangle$
Buckling temperature	184.7	225.6
Weight ratio, $W/W_s$	1.00	1.00

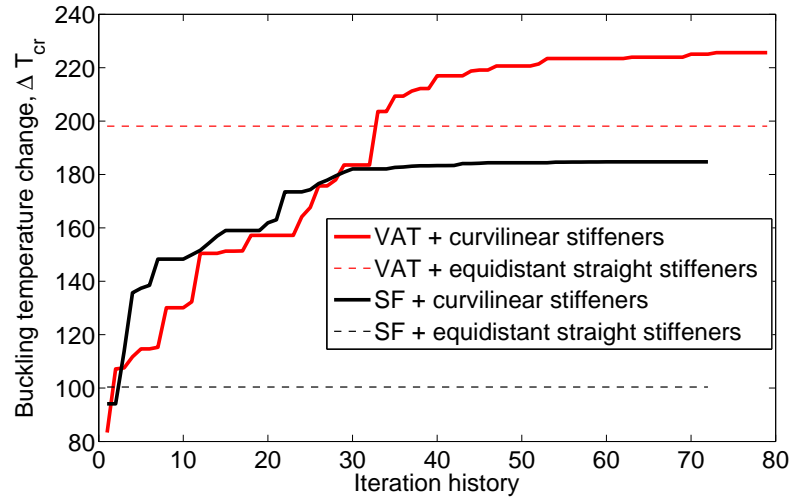


Figure 23: Iteration history of buckling temperature for both cases

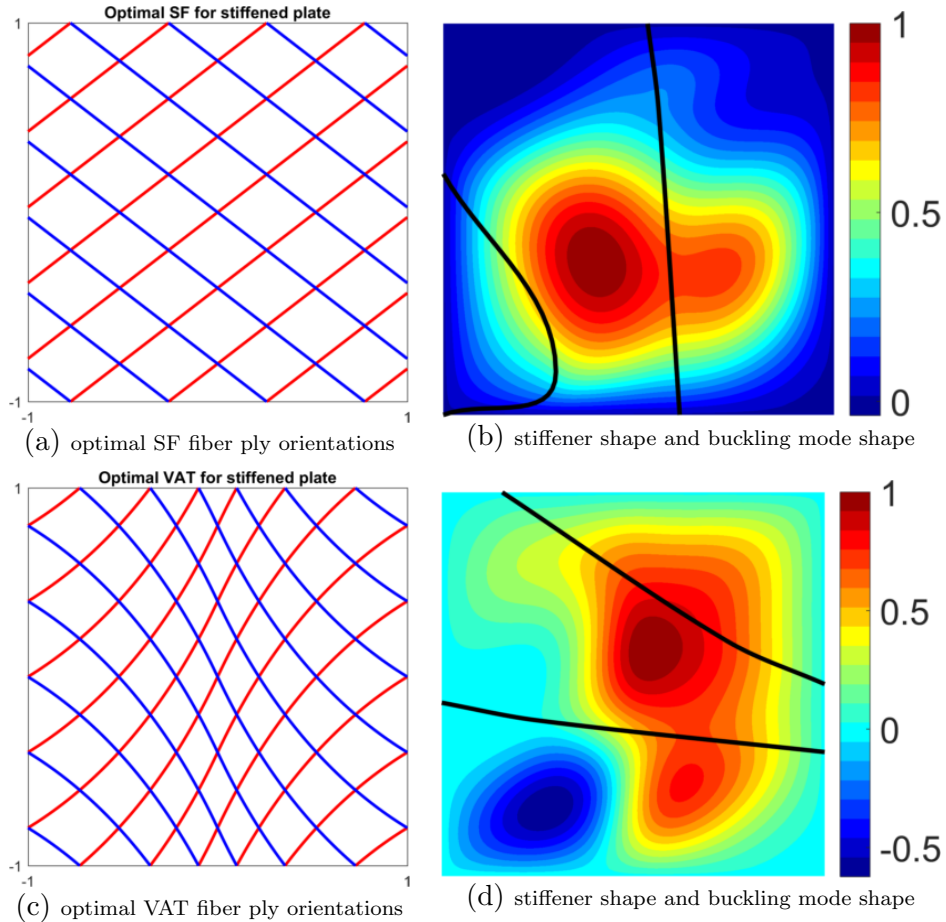


Figure 24: Optimal laminates and stiffeners shape, and buckling mode shapes for straight-fiber and VAT laminate configurations under a uniform temperature change

## VI. Mechanical Buckling of Curvilinearly Stiffened Plates

In this section, we are not going to verify the present program for studying the buckling of stiffened VAT laminates under in-plane loads. This is because our previous work [20, 22] have studied buckling analysis of curvilinearly stiffened composite plate in the presence of both in-plane normal and shear stresses and a stiffened VAT laminated plates subjected to initial displacement and linearly varying in-plane loads.

This section considers the in-plane uniform axial loads as shown in Fig. 25. As compared to the concentric stiffeners, the eccentric stiffeners not only increase the total structural bending stiffness but also increase the axial stress due to the coupling of the in-plane displacement and the out-of-plane rotations when the plate is subjected to in-plane loads [22]. For simplicity, only concentric stiffeners are considered in this section. This section will conduct parametric studies on buckling loads in terms of both VAT laminates fiber ply orientation and stiffener shape. An optimization is then conducted to maximize the buckling load in terms of the VAT laminates and the stiffener shape.

### A. Straight Stiffeners

The geometry model and the material properties studied in Section V-B are used in this section. A uniform in-plane axial load is considered,  $N_{xx} = 1 \times 10^3$  N/m as shown in Fig. 25.

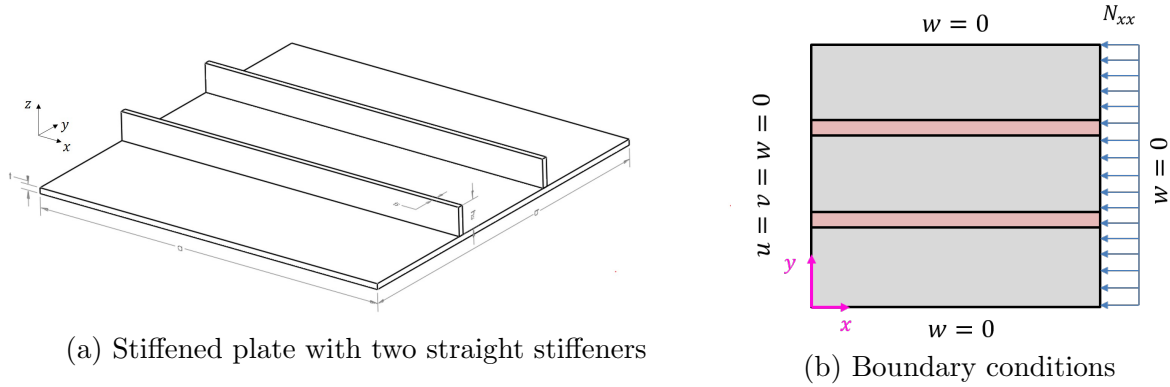


Figure 25: Stiffened plate and boundary conditions

The buckling load for both unstiffened and stiffened plates in terms of different fiber ply orientations in the presence of a uniform in-plane axial load are studied and shown in Fig. 26. It is seen that the VAT laminates can improve the buckling responses for both unstiffened and stiffened plates. The maximum buckling loads and the corresponding optimal straight-fiber and VAT laminate configurations are shown in Table 12. The VAT laminates can improve the buckling load by 17.9% and 9.2%, respectively, for the unstiffened and stiffened plates. The buckling mode shapes corresponding to the optimal configurations for both unstiffened and stiffened plates are shown in Fig. 27.

The buckling mode shapes for the optimal straight-fiber and VAT laminates are similar for the unstiffened and stiffened plates. This is consistent with the findings in our previous

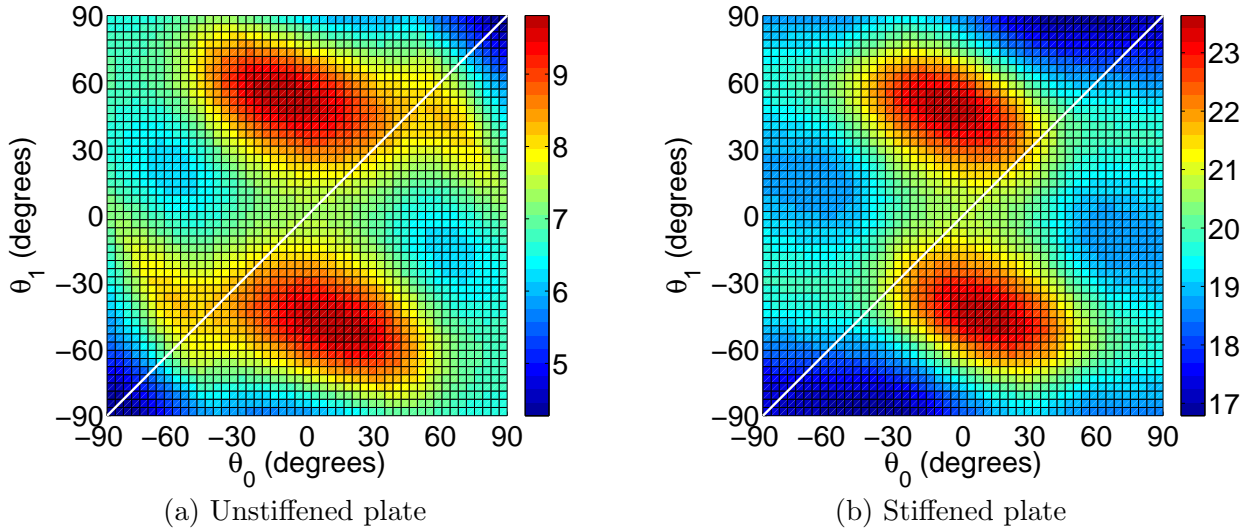


Figure 26: Buckling load of unstiffened and stiffened VAT plates under uniform in-plane loads in terms of VAT laminates fiber orientation

Table 12: Maximum buckling load factor,  $\lambda_{b,cr}$ , for a square VAT laminated panel

Composites	unstiffened plate	stiffened plate
Straight-fiber laminates	8.32 ( $\pm\langle 31.22^\circ   31.22^\circ \rangle$ )	21.64, ( $\pm\langle 23.88^\circ   23.88^\circ \rangle$ )
VAT laminates	9.81 ( $\pm\langle 12.86^\circ   -53.27^\circ \rangle$ )	23.64, ( $\pm\langle 5.51^\circ   -45.92^\circ \rangle$ )
Improvement	17.91%	9.24%

studies [22]. The VAT laminates are mainly used to redistribute the in-plane stress resultants for the structure in the presence of an axial in-plane load for both the unstiffened and stiffened plates with two straight equidistant stiffeners. Considering the capability of tailoring buckling mode shape using curvilinear stiffeners for improving the buckling response, it is possible to use curvilinear stiffeners and VAT laminates simultaneously to further increase the buckling load for composite plates.

## B. Curvilinear Stiffeners

### 1. Parametric study

Figure 28 shows the buckling load with the shape parameter,  $\xi_2$ , in the presence of a uniform axial load. The model employed in this parametric study is given in Fig. 20. The VAT laminate configuration for the plate is  $\langle 5.51^\circ | -45.92^\circ \rangle$ . There are two optimal designs for the curvilinearly stiffened VAT laminated plate as seen in Fig. 28. As compared to the

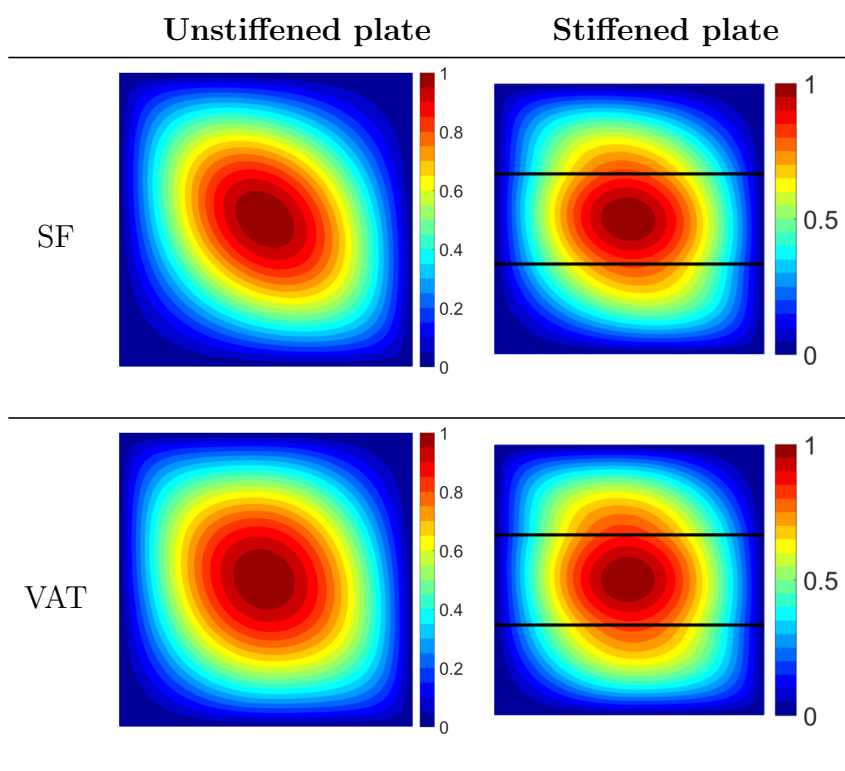


Figure 27: Buckling mode shapes corresponding to the maximum buckling temperature change

responses for the plate with straight stiffeners, curvilinear stiffeners can increase the buckling load by up to 28.2% with a total weight penalty of 5.1%  $W_s$ .

As expected, the discontinuous change of the buckling load with the shape parameter is because the buckling mode shape changes with the shape parameter as seen in Fig. 29. It is clearly seen that the curvilinear stiffeners change the buckling mode shape through modifying the buckling mode wavelength for improving the buckling load.

## 2. Buckling optimization

Similarly, we study two optimization cases for maximizing the buckling load for the plate with straight-fiber laminates and VAT laminates. Both cases consider arbitrarily shaped stiffeners. The optimization problem is summarized as:

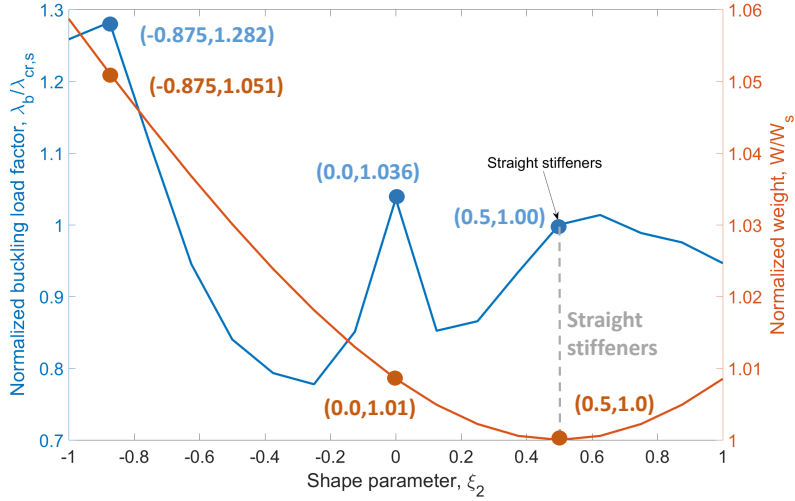


Figure 28: Buckling load with a shape parameter for a curvilinearly stiffened VAT laminated plate under a uniform in-plane load

$$\begin{aligned}
 & \text{maximize} && \lambda_b \\
 & \text{w.r.t.} && \{\Theta_0, \Theta_1, \varepsilon_{1,2}^A, \varepsilon_{1,2}^B, \xi_{1,2}^C, \eta_{1,2}^C\} \\
 & \text{s.t.} && W \leq W_s \\
 & && -90^\circ \leq \{\Theta_0, \Theta_1\} \leq 90^\circ \\
 & && 0 \leq \{\varepsilon_{1,2}^A, \varepsilon_{1,2}^B\} \leq 1 \\
 & && -1 \leq \{\xi_{1,2}^C, \eta_{1,2}^C\} \leq 1
 \end{aligned}$$

The iteration history of the buckling load with generation is shown in Fig. 30. The maximum buckling loads for the two cases and their corresponding stiffener shape and laminate configurations are shown in Table 13. For straight-fiber laminates, the weight constraint is close to 1 while it is active for the VAT laminates. A 27.26% increase in the buckling load is obtained using both VAT laminates and arbitrarily shaped stiffeners as compared to that using straight-fiber laminates. The optimal laminate configurations and the stiffener shapes for each case are shown in Fig. 31. The stiffer shape is being close to straight but in arbitrary placements. It is found that the buckling mode peak is moved from the panel's center to the panel's edge of using both the VAT laminates and the curvilinear stiffeners simultaneously for improving the plate's buckling response.

## VII. Summary

This paper presents an efficient finite element approach for studying buckling responses of stiffened composite panels with both the Variable-Angle-Tow (VAT) laminates and curvilinear stiffeners in the presence of the thermal and mechanical loads. The present method obvi-

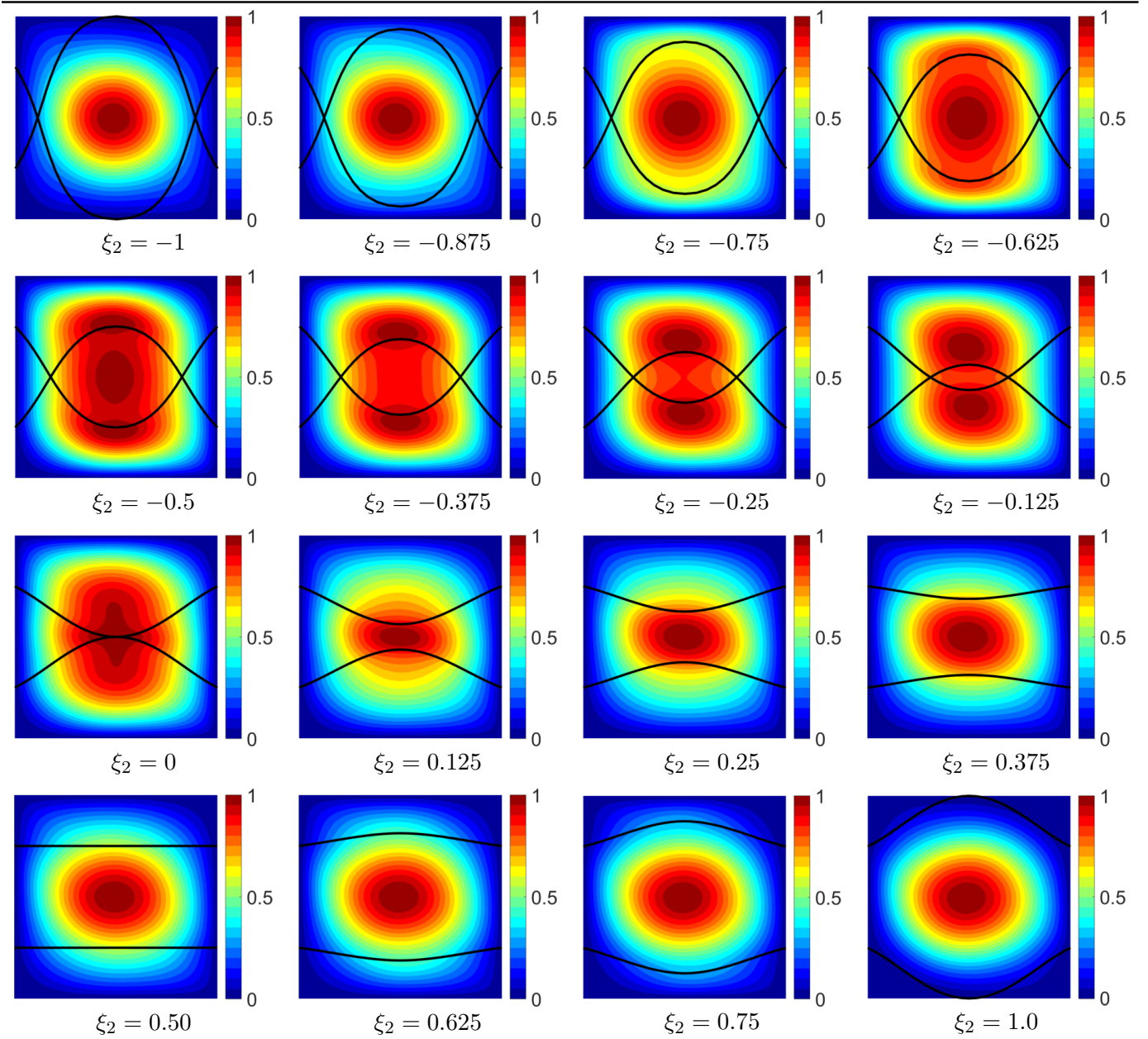


Figure 29: Buckling mode shape for a stiffened plate with different shaped stiffeners

Table 13: Optimal design for the maximum buckling load factor under uniform inplane loads

Composites	Straight-fiber laminates	VAT laminates	
Fiber ply orientation	$\langle 49.56^\circ   49.56^\circ \rangle$	$\langle 89.89^\circ   29.88^\circ \rangle$	
Buckling temperature	118.4	150.67	+27.26%
Weight ratio, $W/W_0$	0.95	1.00	

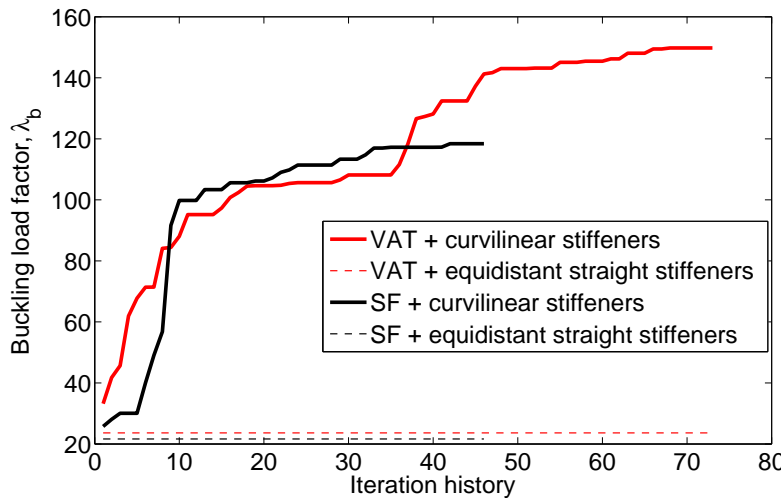


Figure 30: Iteration history of buckling temperature for both cases

ates the requirement to place finite element nodes at the stiffener/plate and stiffener/stiffener interfaces when meshing such structures for structural analysis, which avoids a oft-used relatively fine mesh for the stiffened plate having both spatially dependent fiber ply orientations and arbitrarily shaped stiffeners. Both elastic and geometric stiffness matrices for the beam elements that are used to model the stiffeners are transformed to those of the plate through the displacement compatibility conditions at the stiffener/plate interfaces via finite element interpolation. Since all stiffeners are modeled using composite beam elements, and all the beam element nodal displacements are approximated using that for the plate. The displacement compatibility conditions at the stiffener/stiffener interfaces are satisfied automatically. Convergence and verification studies on the buckling temperatures and buckling loads are studied to demonstrate the accuracy of the present method in buckling analysis of curvilinearly stiffened VAT laminated plates.

Parametric studies on the buckling temperature and the buckling load for both unstiffened and stiffened plates, in terms of the fiber ply orientations, are conducted. The VAT laminates can further improve the buckling responses for the stiffened plate as compared to that using straight-fiber laminates by both redistributing the in-plane stress resultants and tailoring the buckling mode shape. The effect of the stiffener shape on both the buckling temperature

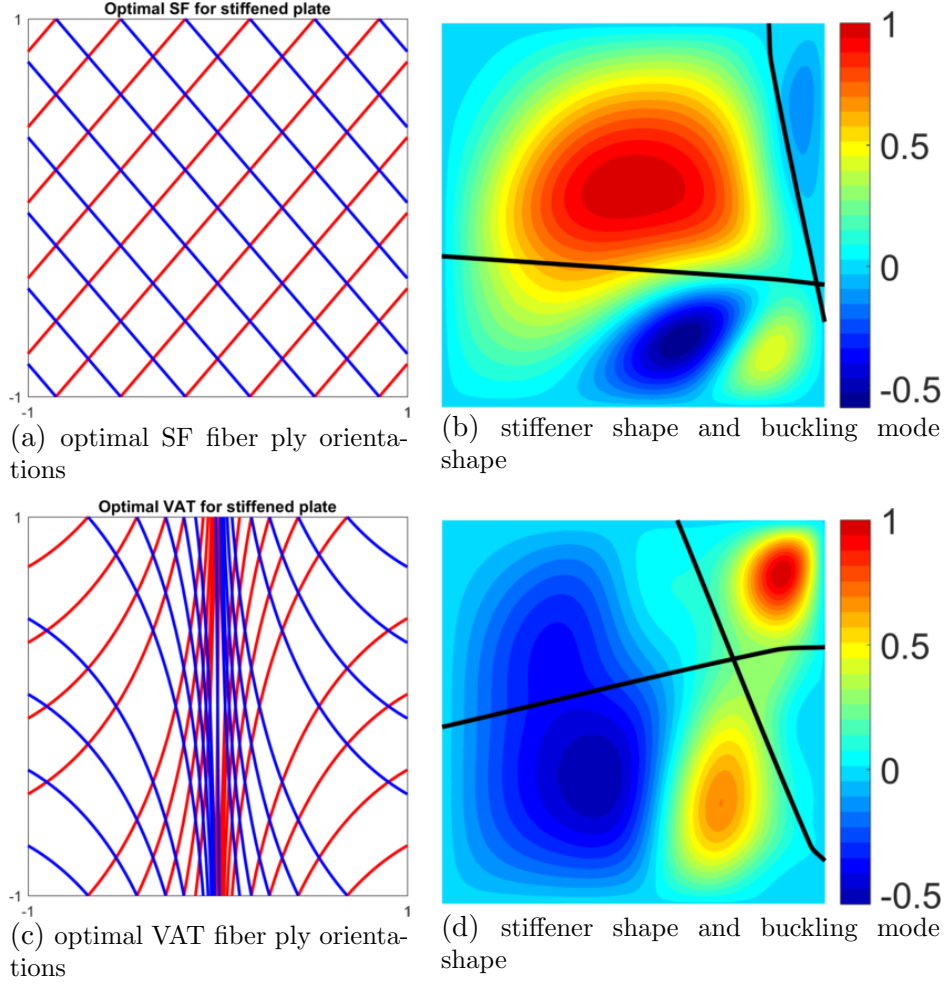


Figure 31: Optimal laminates and stiffeners shape and buckling mode shapes for two cases under mechanical in-plane loads

and the buckling load are studied and parametric study results show that the curvilinear stiffeners are able to tailor the buckling mode shape through modifying the buckling mode wavelength for improving the structural buckling responses.

Considering the capabilities in stress redistribution and mode shape tailoring of using VAT laminates and curvilinear stiffeners, optimization studies on maximizing the buckling temperature and the buckling load are conducted. Optimization results show that using curvilinear stiffeners and VAT laminates simultaneously can further improve the buckling temperature and the buckling load by up to 28% as compared to that using straight-fiber laminates and curvilinear stiffeners. The optimal buckling mode shape is found to be changed by using the VAT laminates and curvilinear stiffeners in modifying the buckling mode wavelength or shifting the buckling mode peak from the panel's center to the place being close to the panel's edges.

## Appendix

### A. The physical coordinates for the stiffener ① in Section V-A is:

$$x = [0, 0.0286719, 0.0573432, 0.0860034, 0.1145922, 0.1432474, 0.1718148, 0.200319, 0.2287029, 0.2569361, 0.2851348, 0.3132083, 0.3411945, 0.3690772, 0.3968614, 0.4246254, 0.4522819, 0.4798695, 0.5073951, 0.5349693, 0.5625];$$
$$y = [0.100, 0.1009157, 0.1018447, 0.1029687, 0.1044766, 0.1065517, 0.1093059, 0.1127888, 0.1169768, 0.1218068, 0.1272279, 0.1331521, 0.1395211, 0.1462728, 0.1533558, 0.1607412, 0.1683552, 0.1761514, 0.1840656, 0.1920529, 0.200]$$

## References

- [1] Thornton, E. A., "Thermal Buckling of Plates and Shells," *Applied Mechanics Reviews*, Vol. 46, No. 10, 1993, pp. 485–506.
- [2] Forster, E., Clay, S., Holzwarth, R., Pratt, D., and Paul, D., "Flight Vehicle Composite Structures," *26th Congress of International Council of the Aeronautical Sciences (ICAS)*, Anchorage, Alaska, 2008, AIAA 2008-8976.
- [3] Gürdal, Z., Tatting, B. F., and Wu, K. C., "Two-Placement Technology and Fabrication Issues for Laminated Composite Structures," *Proceedings of the 46th AIAA/ASME/ASCE/AHS/ASC Structures, Structural Dynamics and Materials Conference*, Austin, Texas, 2005, AIAA 2005-2017.
- [4] Gürdal, Z. and Olmedo, R., "In-plane Response of Laminates with Spatially Varying Fiber Orientations: Variable Stiffness Concept," *AIAA Journal*, Vol. 31, No. 4, 1993, pp. 751–758.
- [5] Taminger, K. M. and Hafley, R. A., "Electron Beam Freeform Fabrication: A Rapid Metal Deposition Process," *3rd Annual Automotive Composites Conference*, Troy, MI, 2003.
- [6] Lee, I., Lee, D.-M., and Oh, I.-K., "Supersonic Flutter Analysis of Stiffened Laminated Plates subject to Thermal Load," *Journal of Sound and Vibration*, Vol. 224, No. 1, 1999, pp. 49–67.
- [7] Chen, L.-W. and Chen, L.-Y., "Thermal Buckling of Laminated Composite Plates," *Journal of Thermal Stresses*, Vol. 10, No. 4, 1987, pp. 345–356.
- [8] Chen, L.-W. and Chen, L.-Y., "Thermal Buckling Analysis of Composite Laminated Plates by the Finite-element Method," *Journal of Thermal Stresses*, Vol. 12, No. 1, 1989, pp. 41–56.

- [9] Meyers, C. A. and Hyer, M. W., "Thermal Buckling and Postbuckling of Symmetrically Laminated Composite Plates," *Journal of Thermal Stresses*, Vol. 14, No. 4, 1991, pp. 519–540.
- [10] Shiau, L.-C., Kuo, S.-Y., and Chen, C.-Y., "Thermal Buckling Behavior of Composite Laminated Plates," *Composite Structures*, Vol. 22, 2010, pp. 508–514.
- [11] Ounis, H., Tati, A., and Benchabane, A., "Thermal Buckling Behavior of Laminated Composite Plates: a Finite-element Study," *Frontiers of Mechanical Engineering*, Vol. 9, No. 1, 2014, pp. 41–49.
- [12] Reddy, J. N. and Chin, C. D., "Thermomechanical Analysis of Functionally Graded Cylinders and Plates," *Journal of Thermal Stresses*, Vol. 21, No. 6, 1998, pp. 593–626.
- [13] Zhao, X., Lee, Y., and Liew, K. M., "Mechanical and Thermal Buckling Analysis of Functionally Graded Plates," *Composite Structures*, Vol. 90, No. 2, 2009, pp. 161–171.
- [14] Duran, A., Fasanella, N., Sundararaghavan, V., and Waas, A., "Thermal Buckling of Composite Plates with Spatial Varying Fiber Orientations," *Composite Structures*, Vol. 124, 2015, pp. 228–235.
- [15] IJsselmuiden, S. T., Abdalla, M. M., and Gürdal, Z., "Thermomechanical Design Optimization of Variable Stiffness Composite Panels for Buckling," *Journal of Thermal Stresses*, Vol. 33, No. 10, 2010, pp. 977–992.
- [16] Gürdal, Z., Tatting, B. F., and Wu, C., "Variable Stiffness Composite Panels: Effects of Stiffness Variation on the In-Plane and Buckling Response," *Composites Part A: Applied Science and Manufacturing*, Vol. 39, No. 5, 2008, pp. 911–922.
- [17] Setoodeh, S., Abdalla, M. M., IJsselmuiden, S. T., and Gürdal, Z., "Design of Variable-Stiffness Composite Panels for Maximum Buckling Load," *Composite Structures*, Vol. 87, No. 1, 2009, pp. 109–117.
- [18] IJsselmuiden, S. T., Abdalla, M. M., and Gürdal, Z., "Optimization of Variable Stiffness Panels for Maximum Buckling Loads using Lamination Parameters," *AIAA Journal*, Vol. 48, No. 1, 2010, pp. 134–143.
- [19] Wu, Z., Weaver, P. M., Raju, G., and Kim, B. C., "Buckling Analysis and Optimisation of Variable Angle Tow Composite Plates," *Thin-walled Structures*, Vol. 60, 2012, pp. 163–172.
- [20] Zhao, W. and Kapania, R. K., "Buckling Analysis of Unitized Curvilinearly Stiffened Composite Panels," *Composite Structures*, Vol. 135, 2016, pp. 365–382.
- [21] Coburn, B. H., Wu, Z., and Weaver, P. M., "Buckling Analysis of Stiffened Variable Angle Tow Panels," *Composite Structures*, Vol. 111, 2014, pp. 259–270.

- [22] Zhao, W. and Kapania, R. K., "Buckling of Stiffened Variable-Angle-Tow Laminates subjected to Nonuniform In-plane Loads," *Composite Structures*, 2018, Under review.
- [23] Stanford, B. K. and Jutte, C. V., "Comparison of Curvilinear Stiffeners and Tow Steered Composites for Aeroelastic Tailoring of Aircraft Wings," *Computers and Structures*, Vol. 183, 2017, pp. 48–60.
- [24] Singh, K. and Kapania, R. K., "Optimal Design of Tow-Steered Composite Laminates with Curvilinear Stiffeners," *2018 AIAA/ASCE/AHS/ASC Structures, Structural Dynamics, and Materials Conference*, Kissimmee, FL, 2018, AIAA-2018-2243.
- [25] Mulani, S. B., Slemp, W. C., and Kapania, R. K., "EBF3PanelOpt: An Optimization Framework for Curvilinear Blade-stiffened Panels," *Thin-Walled Structures*, Vol. 63, 2013, pp. 13–26.
- [26] Caffrey, J. and Lee, J. M., *MSC/NASTRAN 2014 Linear Static Analysis: User's Guide*, 2014, MacNeal-Schwendler Corporation.
- [27] Leiva, H. S. V., *Structural Design Optimization of An Aircraft Composite Wing-box Using Curvilinear Stiffeners*, Fakultät Technik und Informatik, Department Fahrzeugtechnik und Flugzeugbau, 2014, Master's Thesis.
- [28] Singh, K., Zhao, W., Jrad, M., and Kapania, R. K., "Hybrid Optimization of Curvilinearly Stiffened Shells using Parallel Processing," *AIAA Journal of Aircraft*, 2018, Under review.
- [29] Ahlbert, G., *Method Evaluation of Global-Local Finite Element Analysis*, Linköping University, 2012, Master's Thesis.
- [30] Hobby, J. D., "Smooth, Easy to Compute Interpolating Splines," *Discrete & Computational Geometry*, Vol. 1, No. 2, 1986, pp. 123–140.
- [31] Langley, P. T., *Finite Element Modeling of Tow-Placed Variable-Stiffness Composite Laminates*, Virginia Polytechnic Institute and State University, 1999, Master's Thesis.
- [32] Honda, S., Narita, Y., and Sasaki, K., "Maximizing the Fundamental Frequency of Laminated Composite Plates with Optimally Shaped Curvilinear Fibers," *Journal of System Design and Dynamics*, Vol. 3, No. 6, 2009, pp. 867–876.
- [33] Stodieck, O., Cooper, J., Weaver, P., and Kealy, P., "Aeroelastic Tailoring of a Representative Wing Box Using Tow-Steered Composites," *AIAA Journal*, 2016.
- [34] Hyer, M. W. and White, S. R., *Stress Analysis of Fiber-reinforced Composite Materials*, WCB McGraw-Hill, 1998.
- [35] Turvey, G. J. and Marshall, I. H., *Buckling and Postbuckling of Composite Plates*, Springer Science & Business Media, 2012.

- [36] Gürdal, Z., Haftka, R. T., and Hajela, P., *Design and Optimization of Laminated Composite Materials*, John Wiley and Sons, 1999.
- [37] Reddy, J. N., “Mechanics of Laminated Composite Plates: Theory and Analysis, Second Edition,” CRC press, 2004, pp. 132–142.
- [38] Nemeth, M. P., “A Treatise on Equivalent-Plate Stiffnesses for Stiffened Laminated-Composite Plates and Plate-Like Lattices,” 2011, NASA TP-2011-216882.
- [39] Zhao, W. and Kapania, R. K., “Prestressed Vibration of Stiffened Variable Angle Tow Laminated Plates,” *AIAA Journal*, 2018, Under review.
- [40] Oñate, E., “Structural Analysis with the Finite Element Method. Linear Statics: Volume 2: Beams, Plates and Shells,” Vol. 3, Springer Science and Business Media, 2013, pp. 58–62.
- [41] Kapania, R. K., Li, J., and Kapoor, H., “Optimal Design of Unitized Panels with Curvilinear Stiffeners,” *AIAA 5th ATIO and the AIAA 16th Lighter-than-Air Systems Technology Conference and Balloon Systems Conference*, 2005, AIAA 2005-7482.
- [42] Zhao, W. and Kapania, R. K., “BLP Optimization of Composite Flying-wings with SpaRibs and Multiple Control Surfaces,” *AIAA/ASCE/AHS/ASC Structures, Structural Dynamics, and Materials Conference, AIAA SciTech Forum*, Kissimmee, FL, 2018, AIAA 2018-2150.
- [43] Zhao, W., *Optimal Design and Analysis of Bio-inspired, Curvilinearly Stiffened Composite Flexible Wings*, Ph.D. Dissertation, Virginia Polytechnic Institute and State University, Blacksburg, VA, USA, 2017.
- [44] Shi, Y., Lee, R. Y., and Mei, C., “Thermal Postbuckling of Composite Plates using the Finite Element Modal Coordinate Method,” *Journal of Thermal Stresses*, Vol. 22, No. 6, 1999, pp. 595–614.
- [45] Walker, M., Reiss, T., Adali, S., and Verijenko, V. E., “Optimal Design of Symmetrically Laminated Plates for Maximum Buckling Temperature,” *Journal of Thermal Stresses*, Vol. 20, No. 1, 1997, pp. 21–33.
- [46] Liu, Q., Jrad, M., Mulani, S. B., and Kapania, R. K., “Global/Local Optimization of Aircraft Wing Using Parallel Processing,” *AIAA Journal*, Vol. 54, No. 11, 2016, pp. 3338–3348.
- [47] Timoshenko, S. P. and Gere, J. M., “Theory of Elastic Stability,” The McGraw-Hill Book Company, 1963, pp. 225–228.
- [48] Zhao, W. and Kapania, R. K., “Vibration Analysis of Curvilinearly Stiffened Composite Panels Subjected to In-plane loads,” *AIAA Journal*, Vol. 55, No. 3, 2017, pp. 981–997.